

SPIE

The International Society for Optical Engineering



Holographic Nondestructive Testing

T9

John A. Gilbert

University of Alabama in Huntsville

**SPIE/ESD International Symposium on
Optical Engineering and Industrial Sensing
for Advanced Manufacturing Technologies**

Dearborn, Michigan USA
27 June 1988

SPIE (Society of Photo-Optical Instrumentation Engineers)
P.O. Box 10 • Bellingham, Washington 98227-0010

HOLOGRAPHIC NON-DESTRUCTIVE TESTING

by

John A. Gilbert, Ph.D.
Professor and Director of Civil Engineering
Department of Mechanical Engineering/Center for Applied Optics
University of Alabama in Huntsville
Huntsville, Alabama 35899
(205) 895-6029 (205) 895-6154

This tutorial on holographic non-destructive testing covers the governing equations and basic recording techniques used in conventional double-exposure, real-time, and time-average holography. First, the strategy for applying these techniques is discussed; then, advances in the state of the art are presented including practical implementation of all three techniques using various combinations of holocameras, holographic/fiber optic (HFO) recording systems, and computers. Laboratory experiments are suggested, and one approach to the automated analysis of holo-interferograms is covered in detail. The tutorial ends with a discussion of a hybrid approach combining holographic interferometric measurements with finite element analysis.

* * * * *

John A. Gilbert received B.S. (aerospace) and M.S. (applied mechanics) degrees from the Polytechnic Institute of Brooklyn in 1971 and 1973, respectively. His Ph.D. (mechanics) was obtained from the Illinois Institute of Technology in 1975. Upon graduation, he taught at the University of Wisconsin-Milwaukee, and moved to the University of Alabama-Huntsville as Professor in 1985.

Professor Gilbert specializes in experimental stress analysis and applied optics with principal expertise concentrated in the areas of remote sensing through fiber optic systems, holography, high frequency moire, speckle metrology, digital image processing of optically generated fringe patterns, and numerical correlation of speckle data. During the past seven years, Dr. Gilbert has helped to introduce several new ideas into the literature including holographic/fiber optic recording, real-time moire interferometry, ultra-low frequency holography, shadow speckle metrology, radial metrology, line-broadening, and the TAP technique. He received the Distinguished Faculty Award from the UAH Alumni Association in 1988, and holds the 1987 Fellowship Award from the American Society for Nondestructive Testing.

In addition to conducting this research, Dr. Gilbert has acted as scientific advisor to the National Science Foundation, and has served as a technical reviewer for both that agency and the Department of Defense. For the past five years, he has worked as a consultant and resident visitor at AT&T Bell Laboratories in Murray Hill, NJ, and currently works with several technical societies as a tutorial lecturer in the areas of nondestructive testing, and remote sensing through fiber optic systems.

During the past eight years, Dr. Gilbert has served as principal or co-principal investigator on grants and contracts totaling nearly one million dollars. He currently holds grants and contracts from NASA, ARI, and ASNT.

TABLE OF CONTENTS

<u>Description</u>	<u>Page</u>
Cover Page	1
Chapter 1. Holography and Holographic Interferometry	3
1.1 Introduction	3
1.2 Holographic Recording	3
1.3 Holographic Interferometry	4
Applications of Holography	8
Chapter 2. Equations for Holographic Non-Destructive Testing	11
2.1 Phase-Displacement Relations for Double-Exposure and Real-Time Holography	11
2.2 Strategy	17
2.3 Time-Average Holo-Interferometry	20
"A Review of Holographic Techniques for Structural Analysis"	23
Chapter 3. Advances in the State of the Art	26
3.1 Introduction	26
3.2 Holocameras	27
3.3 Holographic/Fiber Optic (HFO) Systems	35
"The Monomode Fiber-A New Tool for Holographic Interferometry"	37
3.4 Holographic/Fiber Optic Experiments	43
3.5 Automated Analysis	47
"Automated Analysis of Holo-Interferograms for the Determination of Surface Displacement"	49
"A Windowing Technique for the Automated Analysis of Holo-Interferograms"	55
3.6 Hybrid Analysis - Combining Holographic Interferometry with Finite Element Analysis	62
Chapter 4. The Future of Holographic Non-Destructive Testing	63
Acknowledgements	65
References	66

HOLOGRAPHIC NON-DESTRUCTIVE TESTING

by

John A. Gilbert, Ph.D.

Professor and Director of Civil Engineering
Mechanical Engineering Department/Center for Applied Optics
University of Alabama in Huntsville
Huntsville, Alabama 35899

CHAPTER 1. HOLOGRAPHY AND HOLOGRAPHIC INTERFEROMETRY

1.1 Introduction

The fundamental concept of holographic recording was demonstrated nearly forty years ago when Dennis Gabor suggested the process as a possible means of improving the resolving power of the electron microscope[1]. It was not until the early 1960's, when Leith and Upatnieks produced the first high quality holographic image using a strong coherent source[2], that widespread attention was given to holography. The exactness of the holographic image made it invaluable for detecting faults, and the holographic recording process[3,4] and holographic interferometry has since become an important diagnostic tool in non-destructive testing[5-9].

1.2 Holographic Recording

Holography is a technique for recording the three-dimensional information of an object on a two-dimensional film plane such that when the hologram is reconstructed or "played back" the original object can be viewed in its original three-dimensional form. The visual effect of looking through a hologram is analogous to looking through a window whose size is defined by the hologram and its relative position to the object.

Two beams of light with a stable synchronized relationship are required

to form a hologram. These beams are conveniently obtained, as shown in Figure 1.1, by splitting the light from a single laser into two parts. One light beam is used as an object wavefront to illuminate the test surface. Light is diffused to the film plate. The other light beam forms a reference wavefront and is directly impingent on the film. Mutual interference between these two highly coherent wavefronts is recorded as a complex diffraction grating. The developed plate is called a hologram and can be reconstructed by illuminating the developed plate with the reference beam (see Figure 1.2). During reconstruction, the original object and associated optics can be completely removed. The reference beam is diffracted by the hologram to form a virtual image of the object.

A good hologram will be recorded provided that the holographic system is properly isolated from unwanted vibrations (mechanical, thermal, etc.), the object and reference beams are approximately equal in length (to within the coherence length of the laser), and that the reference and object wavefronts have common directions of polarization at the hologram (preferably perpendicular to the plane formed by their respective propagation vectors).

TECHNICAL NOTE - CHECK FOR PATHLENGTH, POLARIZATION
AND STABILITY WHEN MAKING A HOLOGRAM.

1.3 Holographic Interferometry

Unlike ordinary photography where only the amplitude of the light intensity is recorded, the holographic process records both the phase and amplitude of the light scattered from an object. Phase information is important, since comparisons of phase (interferometry) provide a mechanism for non-destructive testing.

There are at least three different approaches to doing holographic

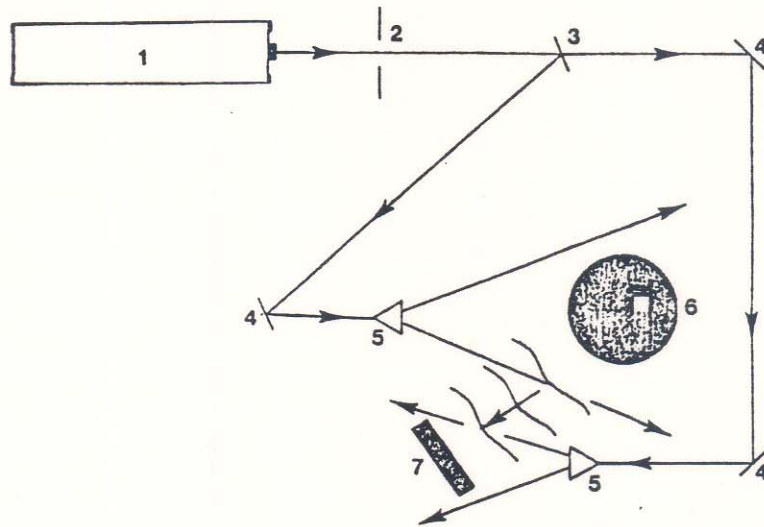


Figure 1.1 Holographic Recording of a Diffusely Reflecting Object.
1. laser; 2. shutter; 3. beam splitter; 4. mirror; 5. spatial filter; 6. object; 7. photographic plate.

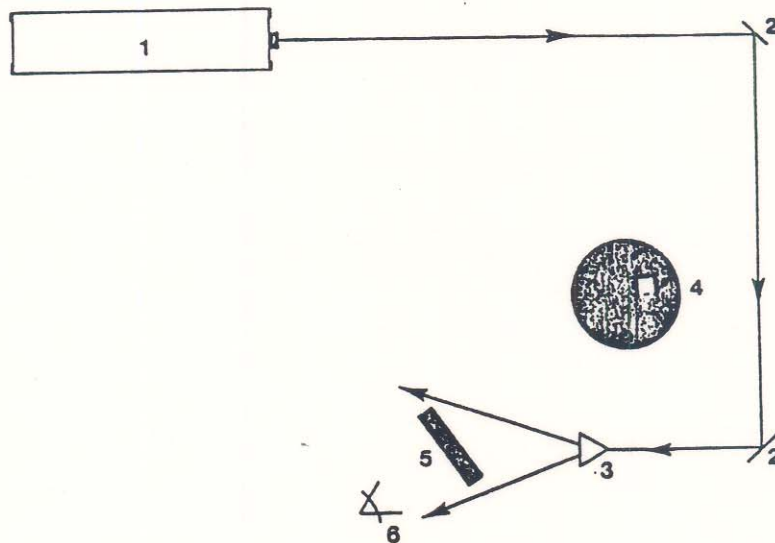


Figure 1.2 Reconstruction of a Hologram. 1. laser; 2. mirror; 3. spatial filter; 4. image; 5. developed hologram; 6. observation.

interferometry, beginning with the time-averaged technique developed by Powell and Stetson[10,11] to reveal contours of constant amplitude on the surface of a vibrating object. In this technique a holo-interferogram is produced by generating a hologram by exposing a film plate for a period of time during which the test object executes many cycles of steady vibration. Quantative analysis and interpretation of the resulting fringe fields revealed that the vibratory nodes correspond to the square of the zero-order Bessel function evaluated at zero, $J_0(0)$; the dark holographic fringes to the zeros of $J_0(Z)$, and the light holographic fringes to its maxima and minima. A second technique, usually referred to as double exposure holographic interferometry, generates a high contrast fringe field by interfering two object wavefronts reconstructed from the same doubly exposed hologram. In this case dark cosine fringes appear in space around the test object. These fringes are associated with the changes in optical pathlength (resulting from changes in the test object occurring between exposures) which in turn induce changes in phase. As such, double exposure holographic interferometry provides a permanent record of the changes which occurred between exposures, but no history of information describing the changes over time as they actually occurred. Real time holographic interferometry, on the other hand, provides a cosine fringe field which changes as the test object changes. Real-time fringes are generated directly by interfering the actual coherent wavefront from the object with a reconstructed holographic "reference" wavefront. In order to generate high contrast real-time fringes, this approach requires that the object illumination and reconstructing reference beams be adjusted to yield object wavefronts of nearly equal intensity and that both beams and the hologram be located in exactly their original positions relative to the test object during reconstruction of the reference wavefront. This latter (most critical)

requirement can be met, though often with some difficulty, by precise repositioning of the hologram after its removal for processing elsewhere, or, more effectively, by processing the hologram in place (in situ processing). In recent years the development of so-called "instant" holographic recording systems has greatly facilitated the latter approach. These devices are described in Chapter 3.

TECHNICAL NOTE - THERE ARE THREE BASIC TECHNIQUES FOR
HOLOGRAPHIC NON-DESTRUCTIVE TESTING:

DOUBLE EXPOSURE - PERMANENT RECORD OF PHASE CHANGE
REAL TIME - TIME HISTORY OF PHASE CHANGE
TIME AVERAGE - COUNTOURS OF VIBRATIONAL AMPLITUDE

Some specific applications of holography and holographic interferometry are listed on the following pages, provided courtesy of Newport Corporation, Fountain Valley, California.

APPLICATIONS OF HOLOGRAPHY

Here are a number of specific examples of industrial applications of holography chosen to give you some feel for how this tool might be adapted to your own needs.

Vibration Visualization

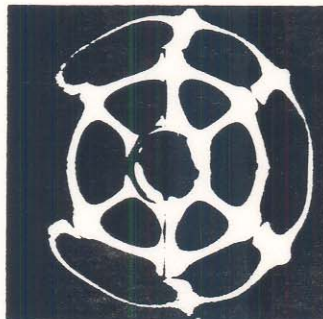
Holography provides a quick way to watch an entire part vibrate, identify its various resonant frequencies, and determine exact vibration amplitudes at any point on the part. You can gain valuable insights into the design of quiet, high reliability equipment by observing the motion of the device as it is vibrated.

Holography has been applied to the design and vibration analysis of turbine blades, rocket casings, pressure vessels, loudspeakers, sonar transducers, automobile engines, bodies, transmissions, gear boxes, rear axles, drive trains, fire walls, gun barrels, vocal cords, transformers,...

Holography is also used to identify the optimum location for attaching a part such as a vibration sensor or a bolt hole, and for inspection to verify that parts are properly bolted or welded together.

Real-time holography is often used to locate resonance frequencies, while time-average holography produces a sharply detailed "modal map" of the vibrating part. Any one of several variations of these techniques may just be the ideal solution for your application.

Surprisingly, this hologram of a vibrating pulley shows that several "bull's eye" patterns, indicative of strong vibration, lie directly on the stiffening ribs.



Deformations Revealed

Holography allows you to see minute submicron deformations caused by small perturbations. Knowing how these minute changes take place can help you in the design or alignment of critical parts, or parts that need to function in adverse environments. In the case of one aerospace guidance control component, for example, holography helped in selecting material to minimize thermal distortions and was also used later in the design stage to determine how to eliminate stress concentrations.

Typically both real-time and double exposure holograms are made when studying deformation of a part. The amount of deformation can be measured directly since the hologram of the part appears overlaid with contour lines which correspond to displacements of 0.15 microns.

Unwanted deformations of a prism mount are immediately apparent from the hologram. The way to redesign the mount to maintain system alignment then became obvious.



Stress-strain Determination

Stress-strain measurements are far more convenient with holography than with alternative methods; they are more precise, and they give more information. No coatings are required on the test object, so no coating related measurement errors can occur. Displacements are measured directly and absolutely, with strain determined by a simple derivative. On average-size objects, surface-strained resolution of one microstrain is typical.

Surface strain induced by the depressurization of this cathode ray tube is determined from the change in fringe spacing. The strain along the line shown in the photograph was measured to be 3.3 microstrains.

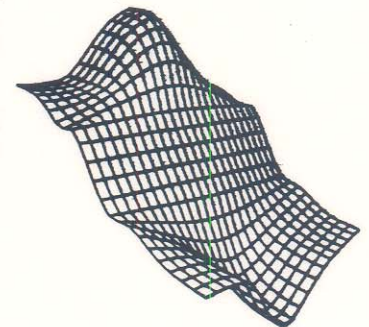


Thermal Strains

It is a simple matter to observe the slightest structural deformations caused by temperature changes even for low coefficient of expansion materials. You can also determine thermal coefficients of materials using test samples of arbitrary shape. With holography, thermal studies are especially easy because no special fixturing or contacting of the test object is necessary.

A dish radio antenna, for example, was continuously monitored as the temperature dropped down to -120°C . Components such as circuit boards, laser housings, and gyroscopes have been checked out holographically during turn-on/warm-up.

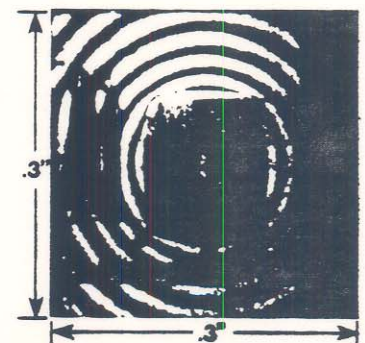
In this case a holographic image has been computer-processed for display with the thermal deformation presented as an exaggerated 3-D map. The item is actually a metal plate with only the tiniest deviations from flatness caused by a slight change in room temperature.



Pressure Effects

Under hydraulic or pneumatic pressure, forces are distributed broadly and thus even simple parts can distort in surprising ways. Valuable engineering data has been obtained by pressurizing and holographically viewing objects such as fuel tanks, food containers, vacuum tubes (depressurization), valves, and flow systems.

Employing holography with microscope magnification, a pressure sensor designer observed exactly how this thin-film resistor array flexed with air pressure fluctuations. Thus they determined the best resistor configuration for maximum sensitivity.



Erosion and corrosion monitored

Holography can, in effect, let you visualize the interior of a pipe. There are several holographic approaches depending on the particular situation. Some are based on comparison of the test object over a period of time, others on instantaneous comparison with an uncorroded sample, with the possibility of using computer processing and display. One procedure is to directly sense the weakening of the pipe walls, another is to sense the flow turbulence caused by corroded surfaces.



The telltale circular fringe pattern indicates weakened regions of the pipe wall. This double exposure hologram was made by introducing slight pressure changes between exposures.

See Invisible Defects

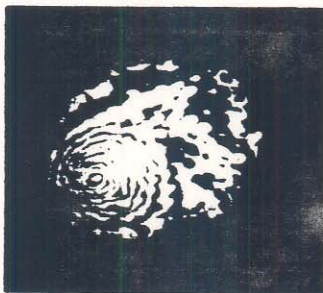
Subsurface or interior irregularities constitute defects if they affect functionality. Since these irregularities show up in the way the material behaves under stress, they can often be detected visually with holographic techniques.

Voids or Debonds Checked

There are several good methods for making subsurface defects visible under holographic scrutiny. One of the easiest is to raise or lower the temperature of the part a degree or two and observe the thermal expansion. Other methods include inducing small pressure changes of tens of millibars, exciting the part in resonance, sweeping the driving frequency, or scattering of impulse-excited propagating waves.

Applications include the inspection of honeycomb panels, composite aircraft components, helicopter rotor blades, clutch plate facings, multilayer circuit boards, tires and o-rings, antique paintings, nuclear fuel rods...

This fault in the bonding between the skin and honeycomb substructure of a composite helicopter rotor blade was revealed by warming the part less than 1°F.



Locating Cracks

There are several ways cracks can be made visible. Since deformation is different near the discontinuity of the crack, the fringe pattern tends to be closely spaced near the crack. Scattering of propagating waves is also effective, along with temperature and pressure changes.

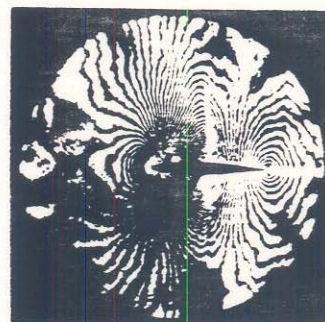
This part was stressed heavily and allowed to relax to check for cracks in the weld seam.



Visualizing Flow

Holography is used in fluid mechanics for flow visualization because it is simple to apply and does not require critical alignment or expensive optics. Holography is also used in plasma diagnostics. Transient events can be recorded with the use of a pulsed laser, or observed through a hologram with a high speed camera.

By calibrating the density at a point far from the airfoil, density over the entire field can be obtained simply by counting fringes in this flow experiment.



Probing with impact pulses

Pulsed-laser holography combined with an impact driver can be used to probe beneath the surface of objects to discover possible flaws. By controlling the synchronization between the impact pulse and the laser pulse, you can track the propagation of the impulse wave throughout the object, and observe how the wave scatters from any irregularities that may exist.

Growth

Study of minute growth of biological samples, crystals, polymer material and contaminants can lead to fundamental understanding. Typically a movie is made of time sequenced holograms of the object.

Holography is used in the skylab to study crystal growth in a zero-g environment. Photo courtesy of NASA.



Microscopy

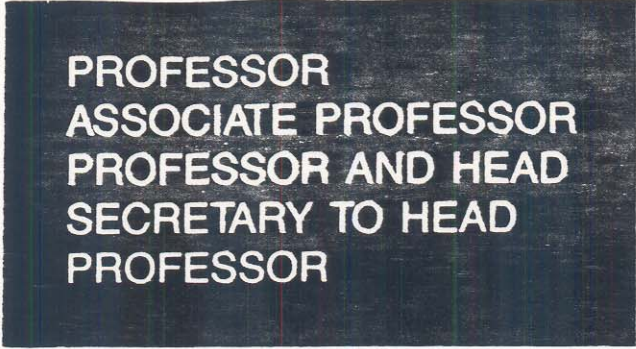
Holographic microscopy allows one to record a whole volume for detailed studies, without being limited by the depth of field of the optical system. Interferometric studies of an object several microns in size are practical.

Hologram of an in vivo marine copepod crustacean recorded with a xenon laser and reconstructed with an argon laser. Photo courtesy of C. Wuerker.



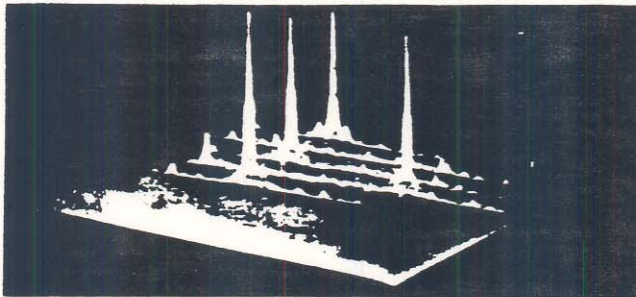
Pattern Recognition

Holographic image processing is a powerful tool, and there is ongoing research to simplify the process for robotics and other commercial applications.

A black and white photograph of a document page with the word 'PROFESSOR' repeated in a grid-like pattern. The text is white on a dark background.

PROFESSOR
ASSOCIATE PROFESSOR
PROFESSOR AND HEAD
SECRETARY TO HEAD
PROFESSOR

(a) Input



(b) Output Correlation

The output of an optical correlator can indicate the presence and location of a reference pattern—for example, the locations of a key word (PROFESSOR) on a page of text. Photo courtesy of D. Casasent.

Process Control

The ability of holography to monitor small changes in physical parameters serves as a basis for applications in process control systems.

Particle Sizing

In addition to density measurements, holographic analyses of particle size distribution and turbulent velocity also yield valuable data for improving combustion efficiency. Holography is also used to analyze pharmaceutical particulate contamination.

Optical Elements

A hologram is like a complicated lens system in that it can convert one beam into a complicated beam and vice versa. Holograms are being used as scanners, filters, diffraction gratings, cockpit heads-up displays, solar concentrators, etc.

Commercial Displays

Three dimensional displays can be impressive conversation pieces. Holography as a graphic art form has been used in applications such as point-of-sale advertising displays.

CHAPTER 2. EQUATIONS FOR HOLOGRAPHIC NON-DESTRUCTIVE TESTING

2.1 Phase-Displacement Relations for Double-Exposure and Real-Time Holography

The general equation presented here provides an adequate but simple basis for the quantitative interpretation of the holographic interference patterns obtained from holo-interferograms. The analysis is limited to measurements of small static displacements on diffusely reflecting surfaces, and is based on the double exposure technique. The same equations govern real time holographic interferometry.

Figure 2.1 shows an arbitrary point P on a diffusely reflecting surface illuminated by a coherent source located at point S. Light with propagation vector \underline{e}_1 is incident on P and is diffused along propagation vector \underline{e}_2 to the observation point O. If a hologram is taken of this "undeformed" configuration and reconstructed, a virtual image of point P is produced when light is diffracted by the hologram back along vector \underline{e}_2 . Before removing the hologram, however, let point P move to a new position P' and allow a second exposure of this "deformed" condition to be superimposed on the first. Light with propagation vector \underline{e}_3 is now incident on P' and is diffused with propagation vector \underline{e}_4 passing through the observation point O. When the developed hologram is reconstructed, propagation vectors \underline{e}_2 and \underline{e}_4 form an interference pattern indicative of the displacement which occurred between points P and P'. This interference pattern is not necessarily localized at the plane of the object[12], but that is of secondary importance in understanding the equations for non-destructive testing.

The phase difference between two neighboring points causes no visible interference pattern to occur because of the random phase differences of the light diffused from these points.

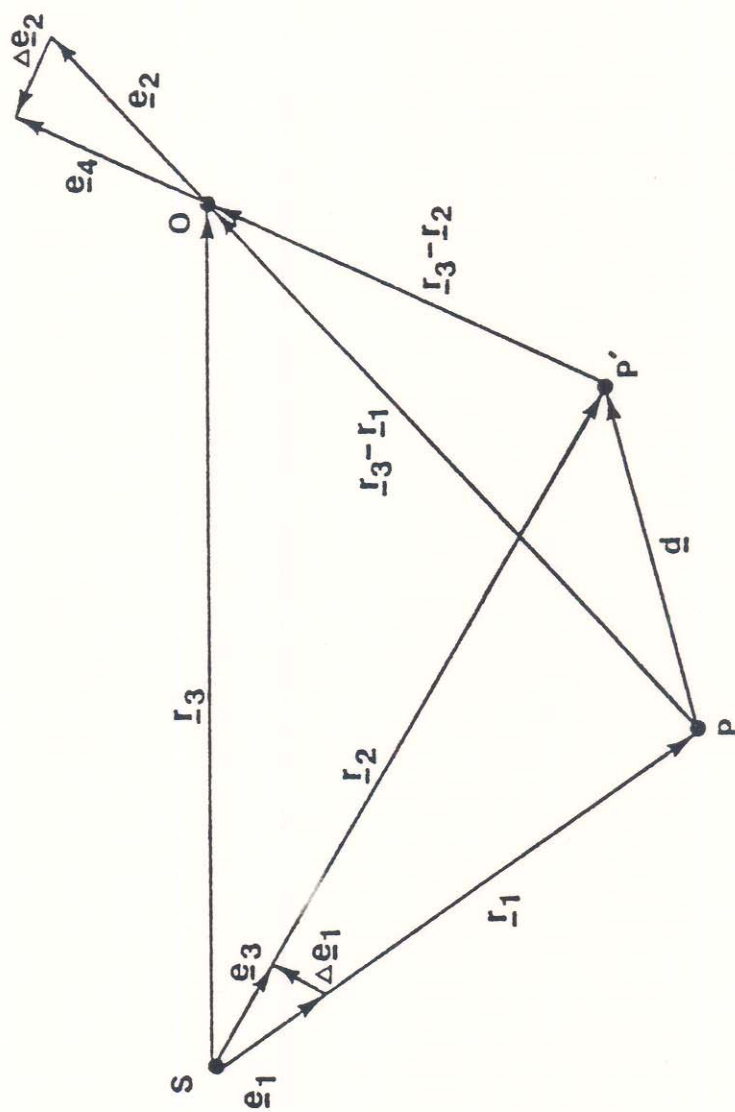


Figure 2.1 Determination of Displacement on a Diffusely Reflecting Surface — General Case.

TECHNICAL NOTE - THERE EXISTS A ONE TO ONE CORRESPONDENCE BETWEEN POINTS ON A TEST SURFACE IN ITS UNDEFORMED AND DEFORMED STATES.

To specify the displacement of point P, it is necessary to determine the phase difference between the paths SPO and SP'O. Letting \underline{r}_1 , \underline{r}_2 and \underline{r}_3 represent position vectors, the angular phase changes δ_1 and δ_2 along the paths SPO and SP'O may be written as

$$\delta_1 = \underline{e}_1 \cdot \underline{r}_1 + \underline{e}_2 \cdot (\underline{r}_3 - \underline{r}_1)$$

and (1)

$$\delta_2 = \underline{e}_3 \cdot \underline{r}_2 + \underline{e}_4 \cdot (\underline{r}_3 - \underline{r}_2)$$

From vector addition

$$\underline{e}_3 = \underline{e}_1 + \Delta \underline{e}_1 \quad (2)$$

$$\underline{e}_4 = \underline{e}_2 + \Delta \underline{e}_2$$

The important quantity is the phase difference $\delta' = (\delta_1 - \delta_2)$. Using equations (1) and (2), this phase difference can be written as

$$\begin{aligned} \delta' &= \delta_1 - \delta_2 = (\underline{e}_1 - \underline{e}_3) \cdot (\underline{r}_3 - \underline{r}_1) \\ &\quad - \Delta \underline{e}_1 \cdot \underline{r}_2 - \Delta \underline{e}_2 \cdot (\underline{r}_3 - \underline{r}_2) \end{aligned} \quad (3)$$

If the magnitude of the position vectors, \underline{r}_1 and \underline{r}_2 , are large as compared to the magnitude of the displacement vector, \underline{d} ; that is,

$$|\underline{r}_1| \approx |\underline{r}_2| \gg |\underline{d}| = |\underline{r}_3 - \underline{r}_1| \quad (4)$$

then $\Delta \underline{e}_1$ and $\Delta \underline{e}_2$ are perpendicular to \underline{r}_2 and $(\underline{r}_3 - \underline{r}_1)$ respectively, and the

corresponding dot products vanish.

Equation (3) can now be written as

$$\delta' = (\underline{e}_1 - \underline{e}_2) \cdot (\underline{r}_1 - \underline{r}_2) \quad (5)$$

Since $(\underline{r}_1 - \underline{r}_2)$ is the negative of the displacement vector \underline{d} , equation (5) can be written as

$$\delta' = -(\underline{e}_1 - \underline{e}_2) \cdot \underline{d} \quad (6)$$

Equation (6) is the general relationship for the determination of the displacement field from an object having a diffusely reflecting surface.

The units in equation (6) are radians which is not a convenient way to express displacement. Accordingly, each propagation vector can be written as

$$\underline{e}_i = \frac{2\pi}{\lambda} \hat{\underline{e}}_i, \quad i = 1, 2, 3, 4 \quad (7)$$

where $\hat{\underline{e}}_i$ is a unit vector along the direction of propagation, $\frac{2\pi}{\lambda}$ is the wave number, and λ is the wavelength of the laser light used to generate the hologram. An interference fringe appears each time δ' is increased by 2π . If n represents the fringe order number at a point in the observed displacement field, then the angular phase difference which occurred during the displacement is $2\pi n$.

Equation (6) can now be written as

$$\delta' = 2\pi n = -(\underline{e}_1 - \underline{e}_2) \cdot \underline{d} \quad (8)$$

or, introducing equation (7)

$$n\lambda = -\left(\frac{e_1 - e_2}{1 - 2}\right) \cdot \underline{d} \quad (9)$$

Equation (9) is the general phase-displacement relation for holo-interferometry written in terms of linear phase.

TECHNICAL NOTE - CHANGES IN OPTICAL PATH MAY PRODUCE FRINGES.
SURFACE DISPLACEMENT IS GOVERNED BY EQUATION (9).

It is desirable to express equation (9) in terms of cartesian coordinates to fully appreciate its consequence and to gain a better physical understanding of the situation at hand. In Figure 2.2, the source coordinates are denoted by (x_s, y_s, z_s) , the observation coordinates are denoted by (x_o, y_o, z_o) , and the surface coordinates are denoted by (x, y, z) . If the displacement vector is given as

$$\underline{d} = U \underline{i} + V \underline{j} + W \underline{k} \quad (10)$$

Then the phase-displacement relation given in equation (9) becomes

$$\left[\frac{x_s - x}{R_s} + \frac{x_o - x}{R_o} \right] U + \left[\frac{y_s - y}{R_s} + \frac{y_o - y}{R_o} \right] V + \left[\frac{z_s - z}{R_s} + \frac{z_o - z}{R_o} \right] W = n\lambda \quad (11)$$

where

$$R_s = \left[(x_s - x)^2 + (y_s - y)^2 + (z_s - z)^2 \right]^{1/2}$$

$$R_o = \left[(x_o - x)^2 + (y_o - y)^2 + (z_o - z)^2 \right]^{1/2}$$

TECHNICAL NOTE - DISPLACEMENT SENSITIVITY DEPENDS ON THE LOCATION OF THE SOURCE AND OBSERVATION FOR A GIVEN MODEL POINT.

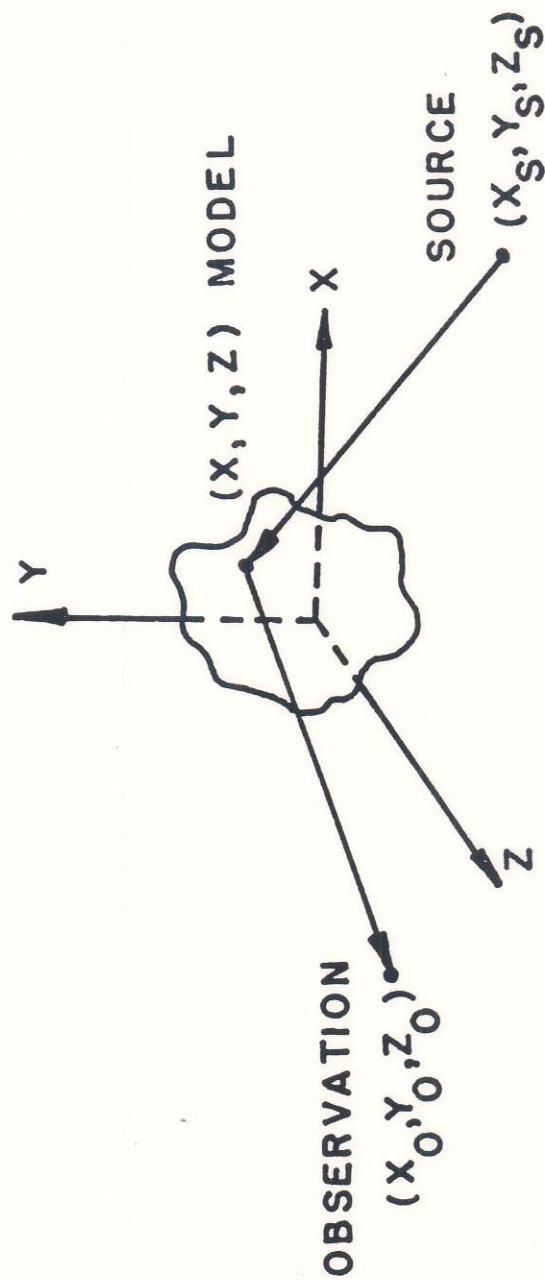


Figure 2.2 Notation for the Cartesian Form of the Governing Equation.

2.2 Strategy

Qualitative evaluation of fringes in holo-interferograms is often sufficient to characterize the problem at hand. The most common techniques for producing fringes for qualitative analysis were given in the examples included in Chapter 1. Quantitative analysis is a different matter.

In general, the displacement vector is projected along a different direction for each model point and it becomes necessary to take several holograms to obtain the necessary information to fully establish the three cartesian components (U,V,W) for every model point. One must change either the source and/or observation point to obtain at least three independent equations in the three unknown displacement components. In practice, it is easier to change the observation direction. Equations are generated when the reconstructed image is photographed from different observation positions located on one or more holograms. A substantial amount of numerical analysis is necessary to analyze this general situation. Data reduction can be minimized, however, by making modifications in the recording and reconstruction phases.

For example, if a relatively flat surface is intentionally oriented normal to the angle bisector of \underline{e}_1 and \underline{e}_2 , the interferometer senses only the out-of-plane displacement component, W, and equation (11) becomes,

$$n \lambda = 2W \cos \beta \quad (12)$$

where 2β is the angle between the propagation vectors in the directions of illumination and observation.

Holographic interferograms can also be optically superimposed to isolate in-plane displacement components. The holographic-moire method is one approach for obtaining such results. In particular, when the object is

illuminated by two beams oriented symmetrically with respect to the surface normal (say each at an angle α), two holo-interferometric fringe patterns result. These are often referred to as component patterns. The fringe orders can be numerically subtracted or the component patterns can be optically superimposed to produce a moire[13,14]. The superposition is characterized by the equation,

$$n \lambda = 2U \sin \alpha \quad (13)$$

where n is the difference between the fringe order numbers in the component patterns, λ is the wavelength used to record and reconstruct the holo-interferograms, and U is the displacement component measured in the plane formed by the propagation vectors from the two sources and oriented perpendicular to their angle bisector.

TECHNICAL NOTE - OPTICS CAN BE POSITIONED TO SELECT A SINGLE DISPLACEMENT COMPONENT TO FACILITATE QUALITATIVE EVALUATION AND/OR QUANTITATIVE ANALYSIS.

In summary, double exposure or real time techniques allow displacements to be measured on tests objects of relatively complicated shape with rather arbitrary surface finish on a scale comparable to the wavelength of light. The holo-interferometric fringes constitute a whole-field display of surface deformation of a test object in response to applied loads. For holographic inspection to work, the deformation of the surface must have an amplitude of about 0.05 micrometers or greater (about one tenth of the wavelength of light). State of the art holographic heterodyning can be used to improve this accuracy to 0.0005 micrometers[15].

The following table summarizes the holographic techniques that are

appropriate for a range of inspection applications. Many small objects can be examined on a vibration-isolated laboratory bench using a continuous wave laser. However, to examine large objects in an industrial environment, pulsed laser techniques are suggested to eliminate unwanted movements that would otherwise wash out the hologram[16].

APPLICATION	HOLOGRAPHIC METHODS	LASER	COMMENTS
Static deflection (strain)	Real-time holographic interference Double-exposure holographic interference	cw cw & p	Small, laboratory experiments. Laboratory and industrial environment. Fringes can be analyzed in detail.
Dynamic deflection (shock loading)	Double-pulsed holographic interference	p	Powerful method of observing unsteady states, fringes can be complex.
Vibration (laboratory tests)	Time-averaged holographic interference	cw	Small components. Detailed information on modes.
	Real-time averaged holographic interference	cw	Lab setup can quickly scan through a large number of modes.
Vibration engineering systems (engines, machinery)	Double-pulsed holographic interference	p	Very powerful technique, can see up to two-meter diameter with high-power laser.
Flaws in rubber tires	Double-exposure holographic interference	cw	Vacuum stressing (flaw expands under vacuum).
Flaws in pipes, cylinders, valves, etc.	Double-exposure holographic interference	cw & p	Apply pressure to interior between exposures.
Honeycomb panels	Double-exposure or time-averaged holographic interference	cw	Stress with pressure, vacuum, or high frequency vibration.
Flaws in composite materials (plates, drum, etc.)	Double-exposure holographic interference	cw & p	Pressure, thermal or vibration stressing.

*As discussed in the text, time-lapse holography can superimpose the images from two holograms, or the image from a single hologram, with the object itself; the latter technique is indicated as "real-time" here. "Double pulsed" indicates time-lapse holography with a lapse of 500 microseconds or less; "double exposure" indicates a larger lapse. The methods summarized here are discussed in detail in the text.

The presence of subsurface flaws such as voids or delaminations can be also be detected, since they perturb the fringe pattern. Here, the key to success is to develop an appropriate means for loading the specimen (mechanical, thermal, pneumatic, acoustic, etc.) such that a defect will cause a detectable anomaly in the deformation pattern.

TECHNICAL NOTE - SUBSURFACE DEFECTS PRODUCE ANOMALIES IN HOLO-INTERFEROGRAMS UNDER APPROPRIATE LOADING CONDITIONS.

It is important to note that holo-interferometric fringes represent absolute phase changes. This often presents a problem, especially when relatively large rigid body motions occur in addition to the deformation. In this case, modulation due to surface strains or subsurface defects may be impossible to detect. Many investigators have approached this problem; techniques include fringe control by reconstructing with two reference beams[17] and the use of sandwich holograms[5]. An alternative is to incorporate optical fibers into the recording system[18]. They can be fixed to a holographic plate carrier to compensate for rigid body motion[19], or attached to a moving assembly to facilitate measurement of the relative motion of components mounted on the assembly. Holographic/fiber optic recording will be discussed in more detail in Chapter 3.

2.3 Time-Average Holo-Interferometry

By observing the photograph of a reconstruction from a hologram of a vibrating object, it is possible to measure the vibration state it had during the recording of the hologram using time average holography[20]. When the exposure time of the recording spans many cycles, the intensity of the reconstructed image is[10,11]

$$I \propto J_0^2 \left[\frac{2\pi}{\lambda} \frac{e}{1} - \frac{e}{2} \cdot \frac{d}{2} \right] \quad (14)$$

This variation is characterized by being a maximum when the argument of the Bessel function is equal to zero, and having succeeding maxima which decrease in value. It can be seen from the plot of the J_0 Bessel function shown in Figure 2.3 that, when the displacement is zero, the reconstructed image is the brightest.

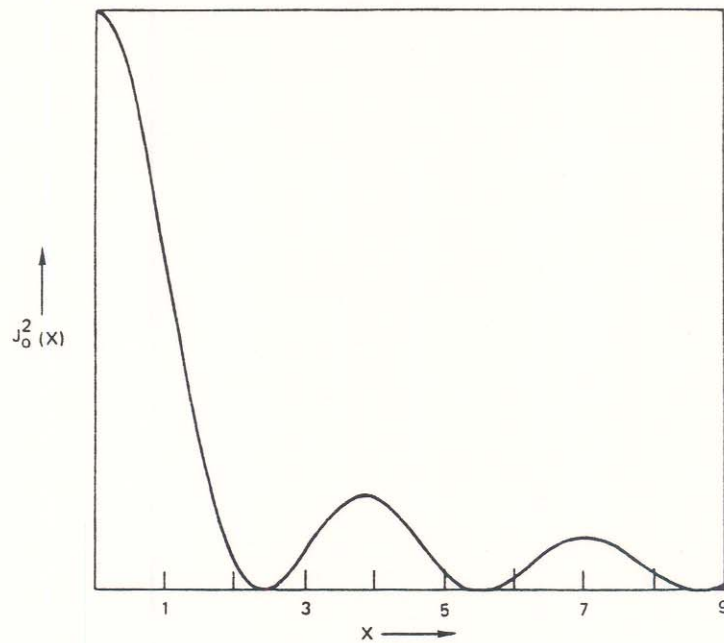


Figure 2.3 Interferometric fringe intensity variation as a result of a cyclic vibratory motion.

Regions having no motion, or nodes in the vibratory pattern, exhibit the greatest intensity and can readily be detected upon inspection of the reconstructed image. Dark fringes occur at the roots (zeros) of the plot; the particular root on the interferogram may be determined by counting from the nearest stationary point on the object, which is marked by the very bright fringe corresponding to the nodal location. The roots of J_0 are tabulated and their values may be used together with the known values of the sensitivity vector to determine the amplitude of object motion in the direction of the sensitivity vector.

If a hologram is recorded of the object while it is vibrating in only one of its vibration modes, then a photograph of the reconstruction from that hologram will display the vibration mode in a simple topographical map of fringe contours. For example, for normal illumination and observation along Z ,

$$N_i = \frac{4\pi W}{\lambda} \quad (15)$$

where W is the displacement component along Z , and N_i are the roots of the Bessel function. This presumes that the sensitivity vector is essentially constant across the surface of the object, and that the vibratory motion is unidirectional. If this is not the case, however, vibration analysis may require more than one holographic perspective per mode[7].

Small amplitude displacement fields can be detected using more sophisticated methods such as phase modulated reference field holography in which a mirror is placed on a transducer vibrating at the same frequency as the object with an amplitude equal to 0.19λ ; or, frequency modulated reference holography where the reference beam is doppler shifted at the same frequency at which the object is vibrating.

Some practical applications of time average holography are included on the following pages in a paper by Rudy Garza and Brad Sharp of Newport Corporation.

A Review of Holographic Techniques for Structural Analysis

Rudy Garza and Brad Sharp, Newport Corporation, Fountain Valley, California

Holographic interferometry techniques are reviewed and applied to structural analysis problems. The procedures benefit finite element modeling, analysis of modal amplitudes, modal analysis of lightweight structures, and modal analysis of complex structures with repeated roots.

Two beams of light with a stable synchronized relationship are required to form a hologram. These beams are conveniently obtained by splitting the light from a single laser into two parts (see Figure 1). One beam is manipulated to illuminate the scene to be recorded and the other illuminates the recording plate directly (reference beam). Light scattered from the scene that reaches the film plate is called the object beam. In order for these two beams to maintain synchronization, they must have traveled nearly the same distance when they reach the film, and must not have been subjected to perturbations such as excess air motion. A hologram is produced when the recording material is exposed and developed. The object beam, or the scene, is completely recreated when the hologram is illuminated with the reference beam.

Holographic Interferometry

Most engineering applications of holography make use of the ability to record two slightly different images and display the minute differences between them. This powerful technique is called holographic interferometry. The ability of holography to recreate 3-dimensional images makes it possible to apply interferometry to 3-dimensional objects. That is, light rays created by the holographic recording medium can be made to interfere with light rays from the real object which generate a set of contour lines. This set of contour lines can be thought of as a topographical map of the deformation, with the elevation between successive contour lines being 12.4 μin . This deformation may be due to minute vibrational, mechanical, thermal or environmental stresses. Holographic interferometry is thus a precise way to determine how an object responds when minute stresses are applied.

Full Field Visualization

A powerful feature of holographic interferometry is that information is obtained from the entire surface of a test object rather than just at a point. The hologram clearly shows those areas of test objects where any kind of activity is occurring. This allows one to identify problem areas quickly in a single operation.

Holographic interferometry supplies the user with much more than a qualitative visual image. The interferometric contour lines provide the precise dimensional data needed for computer aided design and finite element analysis. This is an exciting area of current developmental work which will help the analyst or experimentalist to verify that his computer model accurately predicts the behavior of the actual structure.

Holographic Verification of Finite Element Analysis

Even seemingly straightforward designs can benefit from holographic verification of the results of finite element analysis. A study of the vibration modes of a simple vertically-mounted cantilever beam shown in Figure 2 serves to illustrate this point. Figure 2A shows the modal map of the first bending mode. The node is shown as a light area which is basically the

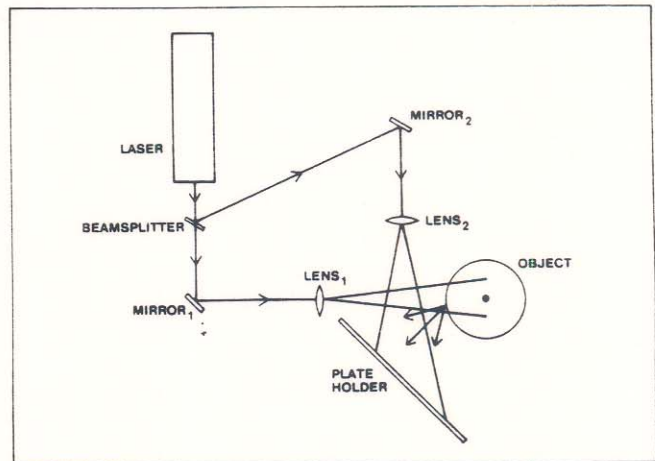


Figure 1. Schematic diagram of holographic interferometry system.

maximum of the Bessel function. The dark fringes each represent an additional displacement coming from the zero-order Bessel function $J_0(Z)$ fringes at $Z = 0$. The first order node of the second bending mode in Figure 2C is clearly seen as the brightest area. Likewise the bright line up the center of the cantilever beam in Figures 2B and 2D is the first order node of the torsional modes. It is important to remember that the nodes represent zero motion, while the fringes indicate peak-to-peak displacement. Modal frequencies calculated by finite element analysis of the cantilever beam were higher than those experimentally observed with holographic testing. The differences are attributed to boundary conditions, modeling assumptions, structural nonlinearities, and other sources of inconsistency.

Determination of Amplitude

In addition to the obvious visualization of mode shapes, the amplitude of motion can be determined. If you are exciting the test object with sinusoidal excitation, the black fringes occur at the zeros of a J_0^2 fringe field (see Figure 3). In order to determine the amplitude of the motion, you simply count the dark fringes from the bright zero order fringe and solve the equation:

$$Z = \xi_n \lambda / 4\pi \quad (1)$$

Z = peak-to-peak vibration amplitude in μin .

ξ_n = zero order Bessel function associated with a given fringe count

λ = laser light wavelength (24.91 μin . for HeNe laser)

If we simplify this equation to the following form, we can calculate the amplitude terms for each fringe as shown in Table 1.

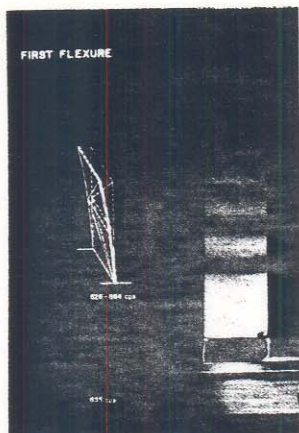
$$Z = 1.9825 \xi_n \quad (2)$$

For a more detailed discussion, refer to *Holographic Interferometry* by Charles M. Vest, published by Wiley and Sons.

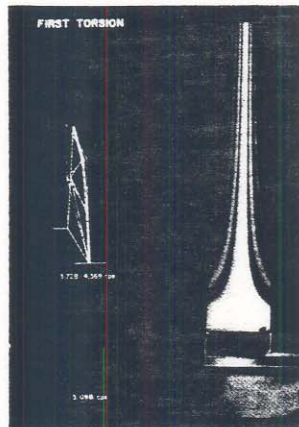
Non-Contact Modal Analysis of a Disk Drive Flexure

In many instances a structure is too small to accommodate the mass loading of an accelerometer without affecting its modal parameters. Holography provides a non-contact way to

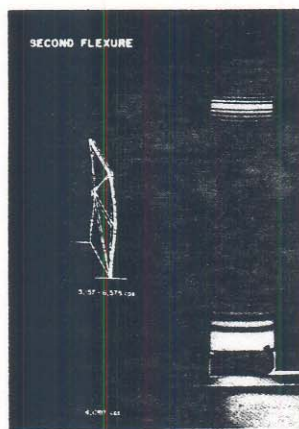
A



B



C



D



Figure 2. Mode shapes for a simple cantilever beam: A. first bending; B. first torsion; C. second bending; D. second torsion.

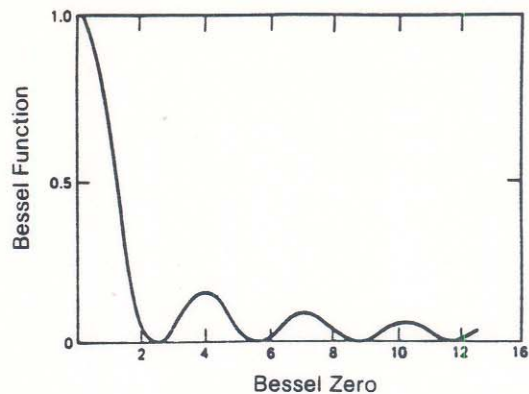


Figure 3. Plot of the J_0^2 Bessel function.



Figure 4. Time average hologram of a disk drive read/write head flexure.

watch an entire part vibrate, identify its various resonance frequencies, and determine vibration amplitudes at any point on the part. The hologram in Figure 4 shows a disk drive head flexure excited at 20,000 Hz. In order to produce a modal map such as this, a time average hologram must be made. To do this a hologram is made while the flexure is being excited with low amplitude vibration. The black and grey fringes represent the areas in motion. The bullseye in the center of the flexure indicates that this area is a breathing mode and the center of the bullseye is an antinode.

Modal Analysis of a Turbine Wheel

Larger objects such as turbine blades and rotors can also be holographically tested. Engineers have found it useful to combine the experimental results of holography with the analytical results of finite element analysis. With holography the operator can get a whole field view of an object's mode shapes yielding precise quantitative measurements of its deformation. If the operator prefers to make his amplitude measurements with accelerometers, then holography can greatly reduce the time typically spent trying to place them by showing the exact locations of maximum deformation. Figure 5A shows a small turbine rotor at 9800 Hz. The mode shape corresponded exactly with the manufacturer's experimentally predicted results. Figure 5B shows the same rotor resonating at the same frequency, but at a slightly higher excitation amplitude. Notice

Table 1. Zeros of the Bessel function J_0 .

Fringe No.	Bessel Zero	Amplitude, μ in.
1.....	2.4048	4.7676
2.....	5.5200	10.9437
3.....	8.6537	17.1564
4.....	11.7915	23.3772
5.....	14.9309	29.6012

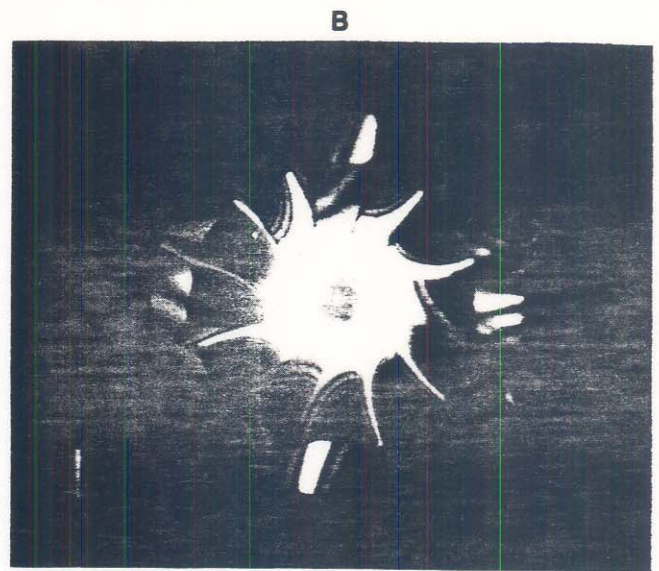
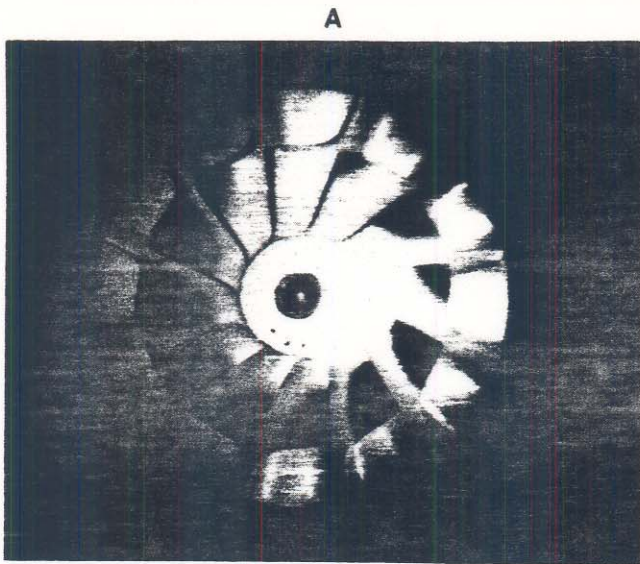


Figure 5. Real time hologram of a small turbine rotor excited at 9800 Hz: A. initial excitation level; B. higher excitation level.

how the base portion has developed a cross-shaped node indicating four-way bending of the casting. Without holography the manufacturer might never have thought to look for this additional information, yet with holography the entire process took about five minutes.

Modal Analysis of a Disk Brake Rotor

Anyone who has driven a car with disk brakes is familiar with the squeal or growl they make while stopping. Figure 6 shows a typical disk brake rotor, while Figure 7 shows the time average hologram of the rotor at 4363 Hz. The modal map is a series of scallop shapes where each scallop represents bending of the rotor edge. The large white node in the center repre-

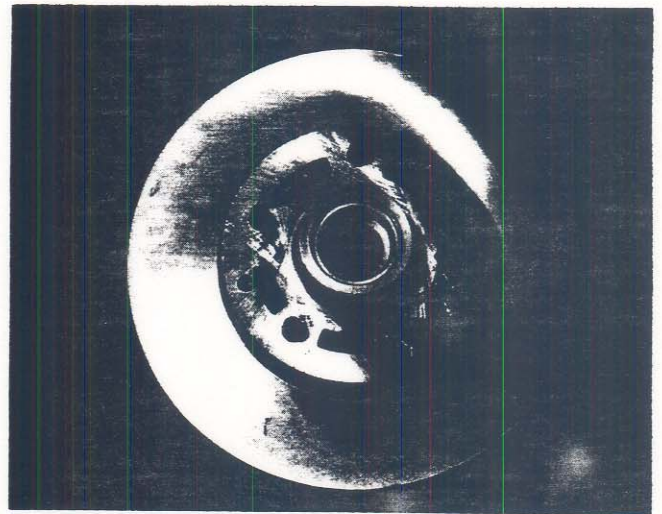


Figure 6. Disk brake rotor.



Figure 7. Time average hologram of a disk brake rotor excited at 4363 Hz.

sents zero motion, and each added fringe toward the rotor's edge is an additional increase in deformation. Maximum amplitude of motion occurs at the rotor's edge, in the center of each scallop shape. With holography a manufacturer can systematically locate and depict any or all of the mode shapes a structure exhibits in a matter of minutes.

CHAPTER 3. ADVANCES IN THE STATE OF THE ART

3.1 Introduction

Conventional continuous wave holo-interferometric systems used to make double exposure, real time, or time average recordings are often limited by stringent vibration isolation requirements and the need for direct optical access to the test surface. Although pulsed laser systems can be used to record highly dynamic events, and consequently do not suffer as greatly from the effects of vibration, they too require direct optical access to the test object and a continuous wave alignment laser and beam splitter for holographic recording. In addition, many holograms are recorded on high resolution photographic plates which must usually be removed from the holographic set-up in order to be developed in a darkroom. For double exposure holo-interferometry, whether pulsed laser or continuous wave, the developed hologram must be reconstructed so that the deformation related fringe pattern can be photographed through the plate using an ordinary camera. Such fringe patterns are most often interpreted "by eye" and analyzed "by hand."

To be useful for displacement analysis in an industrial environment, a holo-interferometric system should be flexible, versatile and self-contained. For example, optics should be easily movable to facilitate the close matching of path lengths (to satisfy coherence requirements) and/or to gain access to a remote test surface. The ability to vary the object illumination and observation directions is desirable to permit measurement of different displacement components, while the ability to vary the angle of the reference beam provides a means of varying the spatial frequency content of the hologram itself. Mechanisms for fixing the illumination and observation positions in order to measure relative movements in three dimensional objects, and for

adjusting the reference illumination position with respect to the hologram in order to compensate for rigid body motion, are also desirable. Fringe patterns should be automatically recorded and numerically processed, etc. Some of these conditions have been met by incorporating fiber optics, holocameras, and electronic image processing into holographic systems. The following sections describe some of these new developments in the state of the art.

3.2 Holocameras

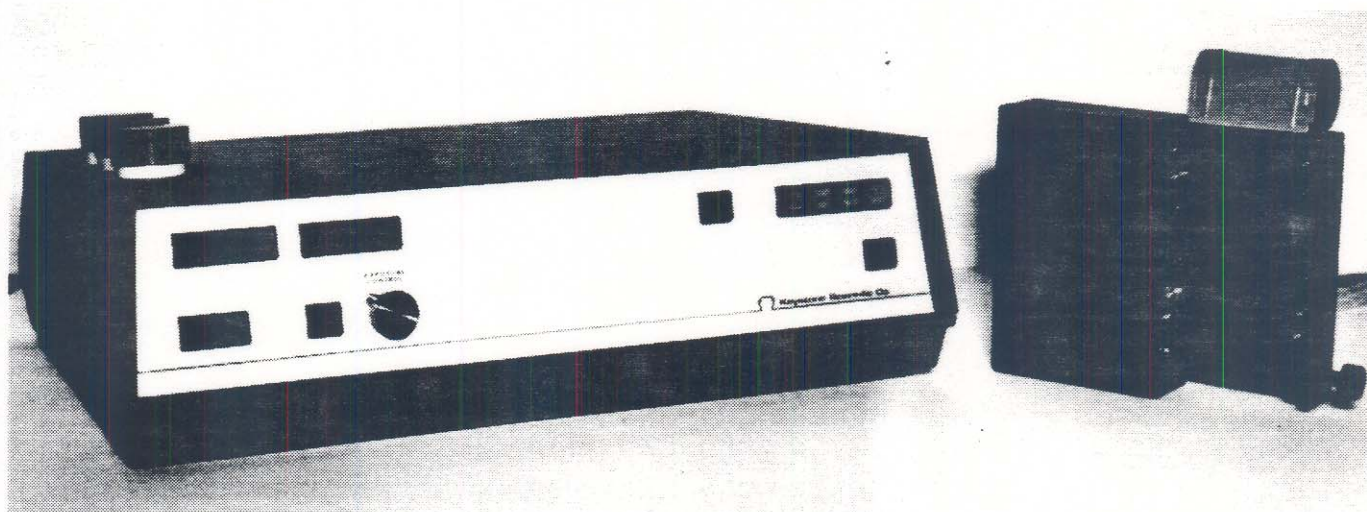
Recent years have seen the development of automated devices called holocameras, capable of recording and processing holograms suitable for real-time interferometry within seconds. There are two basic types of holocameras, those which use widely available high resolution photographic films with silver-halide emulsions and those which use specially manufactured thermoplastic recording materials. Each system has its own advantages and disadvantages. For example, working with silver-halide devices is often a messy affair that may require numerous trial-and-error cycles to produce high-quality holograms. Thermoplastics, on the other hand, can be used to capture only phase information and exhibit high diffraction efficiencies. However, recording is limited to spatial frequencies in the neighborhood of 800 lines/mm, which is unacceptable for ultra-low frequency holography[34]. Additional drawbacks of the thermoplastic device are its relatively high initial cost, and its limited viewing aperture of roughly 3 cm². These drawbacks are partially offset by its reusability and a processing time of one third that required by a photographic film-based system. Both systems are capable of producing bright, clear hologram images for practical real time interferometry, and are described in the following product literature.

AUTOMATIC FILM PROCESSING SYSTEM

Bulletin 862

FOR HOLOGRAPHY, SHEAROGRAPHY, SPECKLE INTERFEROMETRY

- * **IN-PLACE PROCESSING OF STANDARD 35mm AND 70mm FILMS**
- * **STANDARD CHEMISTRY, SINGLE STEP MONOBATH OR D-19/FIXER**
- * **PERMANENT HOLOGRAMS WITH MORE VERSATILITY AND CONTROL THAN ANY OTHER RECORDING SYSTEM AVAILABLE**



**AUTOMATIC
ADJUSTABLE
ADDRESSABLE
AFFORDABLE**

- push button operation
- all operations can be user varied
- all procedures can be user sequenced
- complete system under \$8000

KEYSTONE SCIENTIFIC CO.

P.O. Box 22, Thorndale, PA 19372
(215) 269-2709



GENERAL DESCRIPTION

The most important features in automatic in-place film processors for laboratory use are convenience and versatility, adaptability to a variety of optical set-ups, the ability to use different films and chemistries, minimum maintenance, and of course, economy.

We have met and surpassed all of these criteria. Solid state electronics provide the necessary dependability and versatility - the user has complete control over the sequence and duration of all operations. As an example, the development time cycle for permanent processing can be adjusted from 30 seconds to 3 minutes. All operations can be stopped in cycle, extended, or repeated. You can even vary the duration of each exposure in double or multiple exposure holography.

Compact construction allows maximum access to the film area. Extreme beam angles are possible; beams can also be directed to either or both sides of the film. This same accessibility encourages the use of video and still cameras with large zoom and close-up lenses, while the 70mm format allows direct viewing of the recorded images.

Standard 35mm or 70mm holographic films, with or without dyes or antihalation backings can be used. Processed film can be removed at any time; after each exposure or after the entire cassette has been processed. A processing head using 70mm film will accept 35mm film by simply installing the chamber plate kit - a bolt on accessory.

Standard chemistry and films provide ongoing economies with no concern about availability or compromise in quality. Our policy is to manufacture well-designed systems with the ability to manipulate those systems for a variety of applications.

Each controller and processing head is covered under warranty for one full year. Keystone Scientific Co. is an authorized distributor for Eastman Kodak and Agfa-Gevaert products. See our price list for more information.

This film processing system is the result of many suggestions and discussions with active researchers and technicians over the past years. We are very proud of our accomplishments and welcome any questions or comments you might have.



CONTROLS

ON/OFF - Main power.

RESET - Stops all operations.

DRAIN - Evacuates film chamber of all fluids to allow film advance.
(adjustable pump times from 2 to 10 seconds)

FILM ADVANCE - Indexes fresh film from cassette.
(adjustable from 1.5 to 8 inches)

H2O - Injects water into film chamber to sensitize film and to make film interferometrically stable.
(adjustable pump times from 2 to 10 seconds)

EXPOSURE CONTROL/EXPOSURE - When using Keystone Scientific Co. shutter assemblies with CW lasers, shutters will open for predetermined time. For double exposure holography each exposure can be individually adjusted.
(adjustable times from .7 to 30 seconds)

DEVELOPER - Injects developer, either monobath or D-19, to displace water and start processing time cycle.
(adjustable pump times from 2 to 10 seconds)

PROCESSING - Lamp flashes for predetermined time.
(adjustable from 30 seconds to 3 minutes)

H2O/FIXER - Injects either water or fixer into film chamber to displace developer.
(adjustable pump times from 2 to 10 seconds)

REFERENCE BEAM - Opens reference beam shutter to reconstruct time-average and double-exposure holograms.

OBJECT BEAM - Opens object beam shutter to illuminate object for real time holography.

Indicator lamps monitor fluid levels in reservoirs; Waste reservoir has external drain pump. Intensity of all lighted push buttons and indicator lamps can be adjusted. A switch on the processing head opens the film chamber to load film from cassette.

SPECIFICATIONS

CONTROLLER/DISPENSER

Height	5.5"
Width	19"
Depth	14.5"
Weight	18 lbs.
Voltage	110/60/1 AC 220/50/1 AC (specify)

PROCESSING HEAD

Height	6.5"
Width	8"
Depth	1.7"
Weight	3 lbs.

Specifications and controls subject to change without notice.

ACCESSORIES

(see price list or contact Keystone Scientific Co.
for additional information and film specifications)

CHAMBER PLATE KIT* - To convert processing head to accept additional size films.

MONOBATH DEVELOPER/FIXER - Single step processing fluid for permanent holograms in 30 seconds (Eastman Kodak).

D-19 DEVELOPER - For high resolution processing (Eastman Kodak).

FIXER - For permanent storage of D-19 processed film (Eastman Kodak).

MAGNETIC BASE FOR PROCESSING HEAD - Versatile, stable positioning.

BOLT-DOWN BASE FOR PROCESSING HEAD - Fixed positioning.

SHUTTER ASSEMBLY W/ MAGNETIC BASE - To interrupt HeNe beam.

VIEWER* - To view and photograph holograms from storage.

FILM CASSETTE* - Stores approximately 5 feet of film for use in processing head.

DAYLIGHT FILM LOADER* - loads film into cassettes in room light.

*-Specify 35mm or 70mm

AUTHORIZED DISTRIBUTOR FOR

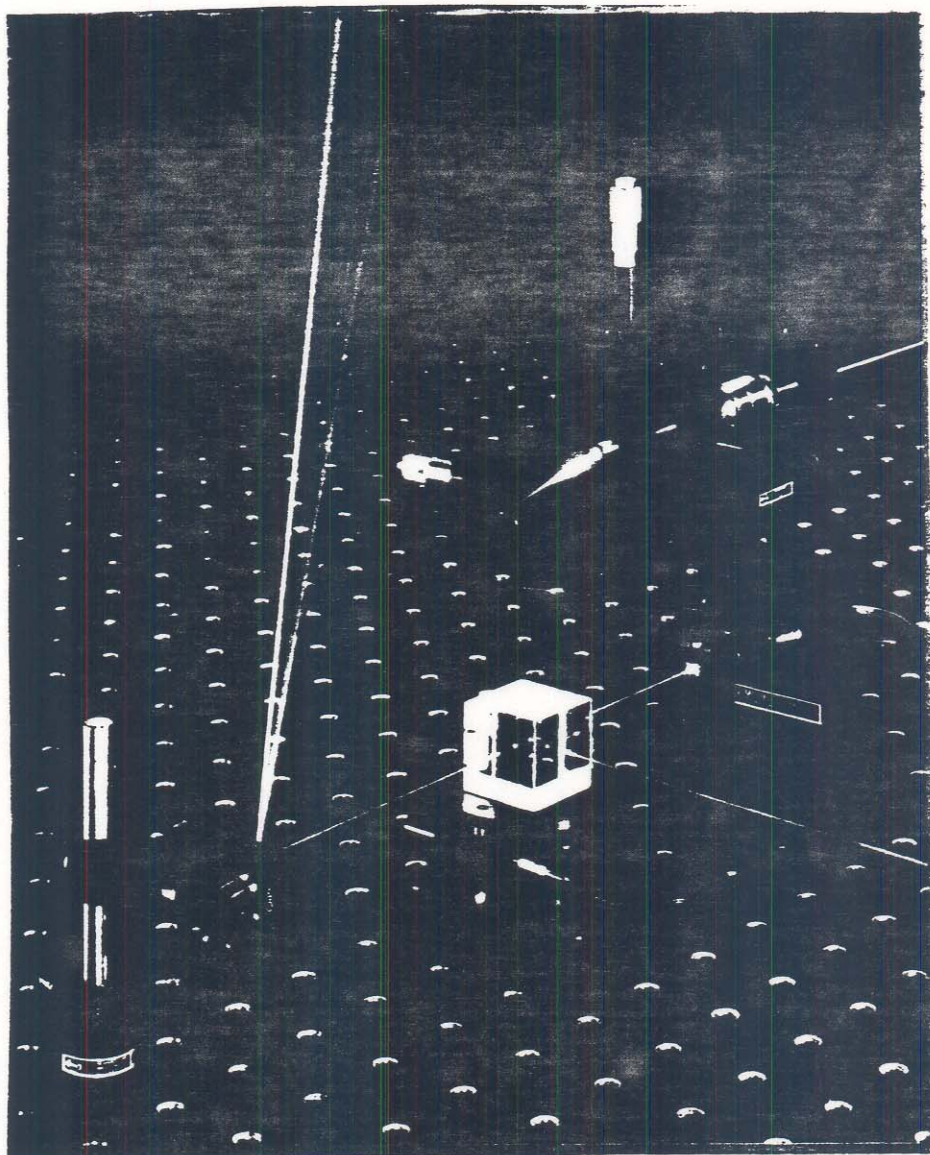
EASTMAN KODAK COMPANY

AGFA-GEVAERT



KEYSTONE SCIENTIFIC CO.

P.O. Box 22, Thorndale, PA 19372
(215) 269-2709

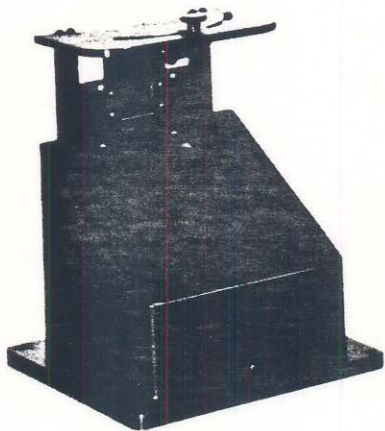


Newport Corporation

POST OFFICE BOX 8020
FOUNTAIN VALLEY, CA 92728-8020
U.S.A.

(714) 963-9811

HC-300 Thermoplastic Recorder



HC-300



The **HC-300** Thermoplastic Recorder is the heart of the **HC-1000** Holographic Camera System.

It has carried the advantages and basic principles of thermoplastic recording to a fully automated system—which is easy to use and rugged enough to function in tough industrial environments.

It is a unique "camera" configuration which can be easily used to upgrade an existing system merely by replacing the present film plate holder, thereby eliminating the long hours and frustration associated with conventional exposure and processing methods.

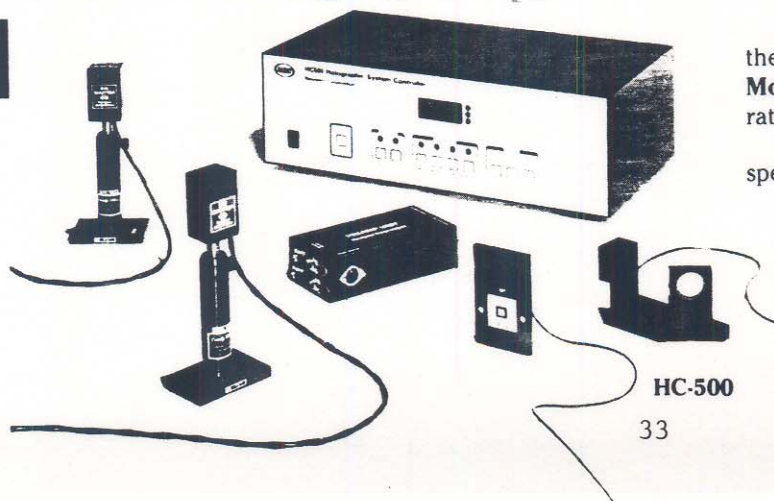
Newport also has an extensive line of **accessories** for all the HC holographic systems. These include video systems, shaker systems and other vibration testing components, an environmental chamber, and optical accessories. These are briefly described at the end of this Holography Section. Details may be found in our new Holography Catalog.

Specifications

Development Time	10 seconds
Development Control	Automatic compensating time makes exposure time noncritical.
Aperture	Sensitized area: 30 mm square.

Sensitivity	About 100 ergs/cm ² at 632.8 nm to reach 7% diffraction efficiency. (The material is substantially faster at shorter wavelengths.)
Optical Bandwidth	Optimized at 800 cycles/mm. (For HeNe lasers, the object/reference angle should therefore be about 36°, and the object should fall within a 20° cone angle in front of the thermoplastic plate.)
Image Life	Once developed, the images are permanent until erased by the unit.
Usable Life	HC-301 Thermoplastic Plate specifications are guaranteed for 300 holograms. (The HC-301 plate has been used successfully for more than 1,000 exposures.)
Cycle Time	Less than 50 seconds—the complete cycle time from erase to viewing the hologram (exclusive of exposure time). The hologram is ready for viewing 10 seconds after the exposure is complete.
Spectral Response	350–700 nm (ultraviolet to infrared).

HC-500 Holographic System Controller



HC-500

The **HC-500** Holographic System Controller operates the HC-300 Thermoplastic Recorder. It also controls two **Model 846** shutters, measures the reference to object beam ratio, and determines the exposure time.

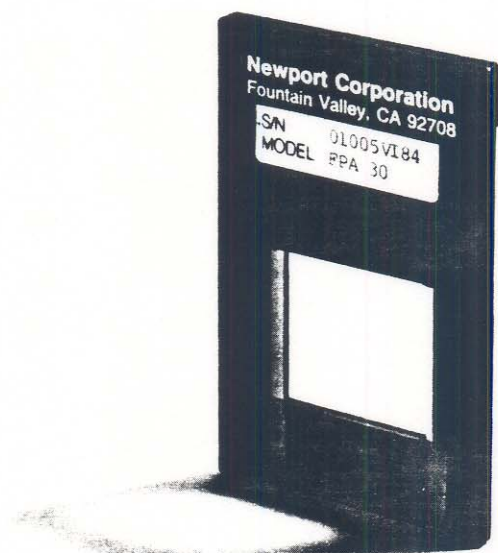
Please refer to the Holography Catalog for detailed specifications of the HC-500 Controller.

HC-301 Thermoplastic Plate

The Newport thermoplastic holography system completely eliminates wet chemical processing. Whether you consider *response*, *access time*, *convenience* or *cost*, the Newport system comes closest to the ideal holographic recording material for design, analysis, and testing applications.

The **HC-301** Thermoplastic Plate is used in the **HC-300** Thermoplastic Recorder (Camera). It is a 1 inch-square, thermoplastic material on a fused silica substrate. It is guaranteed to produce high quality holograms for up to 300 exposure/erasure cycles. This feature makes the HC-301 very attractive in terms of cost per shot, when compared to traditional holographic film.

As an integral part of the HC-300 Thermoplastic Recorder, the specifications for the HC-301 Plates are detailed in the specifications for the HC-300 on the preceding page.



HC-301

Principles of Operation

The HC-301 Thermoplastic Plate is a transparent laminate of four layers: glass substrate; transparent heating element; a photoconductor; and the thermoplastic material. The five steps in a typical operation cycle are shown below: charging, exposure, second charging, development, and erasure.

Charging: A uniform charge is deposited on the thermoplastic and photoconductor.

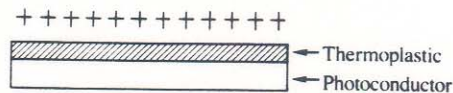
Exposure: Exposure to laser fringe pattern redistributes the charges through the photoconductor.

Second Charging: Recharging increases the electric field across the exposed area of the thermoplastic.

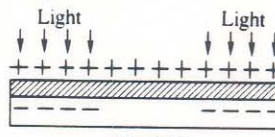
Development: Heating of thermoplastic causes permanent deformation. The irregularities will diffract light to recreate the original image.

Erase: Erasure is done by controlled heating.

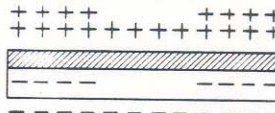
Charging



Exposure



Second charging



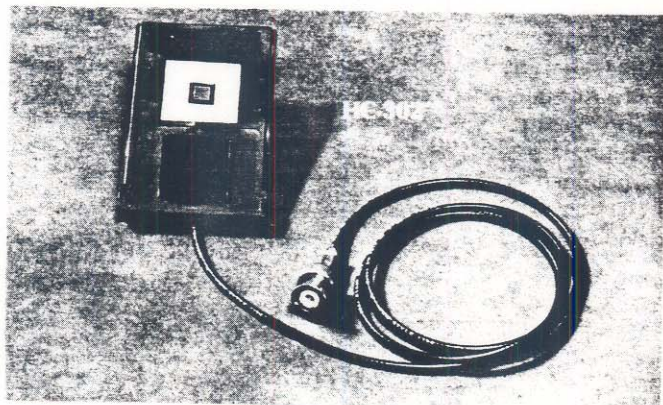
Development



Erase



HC-302 Detector



The **HC-302** Detector is used to determine the beam ratio and approximate exposure for the HC-301 Thermoplastic Plate.

It is composed of a silicon photocell, attached to a BNC cable and mounted on a base plate. The plastic base plate is designed such that it slides into the HC-300 camera head to occupy the normal operating position of the HC-301 Plate. In this position, the exact beam ratio and approximate intensity readings can be taken for the highest quality holographic images.

3.3 Holographic/Fiber Optic (HFO) Systems

Over the last decade, the work of various investigators has demonstrated the practicality of using fiber optic elements for holography[21-27] and holographic interferometry[28-41]. Experience has established that individual single mode fibers provide convenient, highly stable illuminators for holographic interferometry[30,40], while lensed fiber optic bundles may be used to transmit holographic "images" for recording and analysis at locations remote from the actual test objects[29]. Moreover, unlensed fiber optic bundles and individual fibers may be used as flexible illuminators for pulsed laser holography[27] and interferometry[41]. Individual optical fibers and coherent fiber optic bundles may be used in both local and remote holographic systems, including double exposure[32], time average[36], and real time[38] holographic interferometry. Optical fibers can be fixed with respect to the object or hologram to measure relative displacements[19], and can be used to penetrate optically unstable interfaces which are encountered, for example, in making holo-interferometric measurements on the surface of a submerged object[32].

Unfortunately, complete success for holographic/fiber optic recording is not yet here. The need to transmit an image requires a coherent fiber optic image bundle. Since all such bundles presently available are constructed from thousands of fine multimode optical fibers, they are significantly less stable (for holographic applications) than are the SMFs used for illumination. This means that, with any combined single and multimode fiber optic holography system wherein the coherent multimode fiber bundle (MMB) must transmit both amplitude and phase information, considerable care must be taken to secure the full length of the MMB against the deleterious effects of mechanical movement or vibration. Otherwise, such motions produce changes in the MMBs modal

propagation characteristics during recording which degrade or completely eliminate the hologram. Even the use of short exposure durations, as with a pulsed laser, cannot be expected to provide much relief when doing interferometry for all except those events which occur on a time scale shorter than that of the offending MMB disturbances. Fortunately, however, the writer is currently working with a coherent single mode bundle, and it is only a matter of time before it becomes commercially available, allowing tests to be performed on remote objects using rugged, compact holographic probes.

On the other hand, mixed mode holographic systems which do not entail the transmission of phase information via the MMB, such as remotely generated holograms of ultra-low spatial frequency (ULF holograms), are quite stable and effective for both holography and holographic interferometry[34].

TECHNICAL NOTE - USE SINGLE MODE FIBER (SMF) FOR STABILITY.

The following paper[30] discusses single and multimode fibers, and includes more details on holographic/fiber optic recording for non-destructive testing.

The Monomode Fiber—A New Tool for Holographic Interferometry

Monomode and multimode fibers with step-index profiles are used as tools to measure surface displacement by holographic interferometry

by J.A. Gilbert, T.D. Dudderar, M.E. Schultz and A.J. Boehnlein

ABSTRACT—Monomode fibers are used to minimize modal interactions which ordinarily occur during holographic deformation studies based on multimode fiber-optic access. Test results show that holograms have better diffraction efficiency than those generated using multimode fibers and that stringent requirements for vibration isolation associated with holographic testing can be somewhat relaxed.

List of Symbols

a = radius of plate
 a_j = modal amplitude
 d = displacement vector
 d_i = inner diameter of pipe
 d_o = outer diameter of pipe
 \hat{e}_i = unit vector in the direction of propagation
 e_j = modal field
 h = thickness of plate
 n = fringe-order number
 n_{cl} = index of refraction of cladding
 n_{co} = index of refraction of core
 r, θ, Z = cylindrical coordinates
 x, y, z = Cartesian coordinates
 E = Young's modulus
 E, E_B, E_U = propagation modes
 L = length of pipe
 MMB = coherent multimode fiber bundle
 M_T = applied torque
 NA = numerical aperture
 P = applied load
 SMB = coherent monomode fiber bundle
 U_θ = tangential component of displacement
 V = dimensionless waveguide parameter
 W = displacement component along the line of sight
 β_j = propagation constant
 Δ = core to cladding index difference
 θ_c = critical angle

λ = wavelength
 ν = Poisson's ratio
 ρ = radius of fiber core
 $\phi(Z)$ = angle of twist
 ω = angular velocity
 ℓ = length of fiber

Introduction

There has been a great explosion in fiber-optic technology in recent years because of the growing interest in the application of fiber optics to communication systems.¹ Research on optical fibers has now progressed to the point where low-loss fibers suitable for practical non-communications applications have become readily available; however it is essential to evaluate which types of fibers are best suited for which purpose and to design appropriate optimized systems. This paper deals with fundamental advantages of and problems associated with the application of a monomode optical fiber to holographic interferometry.

Fiber Optics

Light can be forced to travel through a thin-glass fiber whose cross section and optical properties are designed based on the phenomenon of total internal reflection. Two of the most common fibers commercially available are graded index and step index. The graded-index fiber is produced so that the index of refraction decreases as the distance from the axis of the fiber increases, while a step-index fiber consists of a core, with refractive index n_{co} , surrounded by a cladding of lower refractive index, n_{cl} . In a step-index fiber, light traveling through the core is reflected back from the cladding provided that the angle of incidence is less than the critical angle, θ_c , defined by

$$\theta_c = \cos^{-1}(n_{cl}/n_{co}) \quad (1)$$

Step-index fibers are used in this investigation.

The numerical aperture (NA), or acceptance angle, of a step-index fiber is given by

$$NA = n_{co}(2\Delta)^{1/2} \quad (2)$$

where Δ is the relative index difference between the core and the cladding defined by

J.A. Gilbert (SESA Member) is Associate Professor, Department of Civil Engineering, University of Wisconsin-Milwaukee, Milwaukee, WI 53201. T.D. Dudderar (SESA Member) is Member, Technical Staff, Bell Laboratories, Murray Hill, NJ 07974. M.E. Schultz and A.J. Boehnlein are Research Assistants, Department of Civil Engineering, University of Wisconsin-Milwaukee, Milwaukee, WI 53201.

Paper was presented at 1982 SESA Spring Meeting held in Oahu and Maui, HI on May 24-28, 1982.

Original manuscript submitted: October 26, 1981. Authors notified of acceptance: June 15, 1982. Final version received: August 15, 1982.

$$\Delta = \frac{n_{co}^2 - n_{cl}^2}{2n_{co}^2} \quad (3)$$

Step-index fibers which have a large numerical aperture, or acceptance angle, are classified as multimode. In addition to rays or modes traveling straight through the fiber, some trace coarse zigzag paths down the guide. The electric field along the fiber can be written in terms of the modes of the system as²⁻⁵

$$\underline{E} = \underline{E}_B + \underline{E}_U \quad (4)$$

where \underline{E}_B represents a finite number of bound modes which in an ideal, nonabsorbing fiber propagate with no change or attenuation, while \underline{E}_U represents an integral that includes all energy which, even for an ideal fiber, leaves the core and radiates into the cladding.

For light of angular frequency ω , propagating through the fiber in the z direction,

$$\underline{E}_B = \sum_{j=1}^N a_j \underline{e}_j(x, y, \beta_j) e^{i(\omega t - \beta_j z)} \quad (5)$$

where a_j , \underline{e}_j and β_j are the modal amplitude, modal field and propagation constant for mode j , respectively. The modal amplitude is determined by the source exciting the fiber while the modal-propagation constants are a function of the dimensionless waveguide parameter, V . The latter can be defined in terms of the indices of refraction, the fiber-core radius, ρ , and the light wavelength, λ , as,

$$V = \left(\frac{2\pi\rho n_{co}}{\lambda} \right) \left(1 - \frac{n_{cl}^2}{n_{co}^2} \right)^{1/2} \quad (6)$$

Generally speaking, the modes propagating in an optical fiber can be uniquely and completely defined through the two parameters ρ and V . The number, N , of bound modes which propagate in a step-index fiber depends monotonically on V ; and, when V is large, $N \approx \frac{1}{2} V^2$. For example, hundreds of modes propagate along fibers with $V > 20$. Each mode propagates with a different group velocity and modal dispersion occurs along the fiber.⁶ Although spatial coherence is practically preserved in each wavefront transmitted through the fiber, detrimental modal interaction can be extremely severe when the fiber is applied to holographic interferometry.^{7,8}

Intermodal dispersion decreases when the dimensionless waveguide parameter, V , becomes small, and a step-index fiber is classified as monomode when $V < 2.405$. In this case, only one mode propagates through the fiber and intermodal dispersion is minimized.⁹

For a given wavelength, eq (6) shows that V can be decreased by minimizing the difference in refractive indices of the core and cladding and/or decreasing the fiber diameter. A small fiber diameter increases difficulty in launching and joining; therefore, a practical step-index, monomode fiber can be manufactured most simply by combining materials with very similar refractive indices. Fibers of this type are called weakly guiding¹⁰ and the relative index difference, Δ , defined by eq (3), becomes

$$\Delta = \frac{n_{co} - n_{cl}}{n_{co}} \quad (7)$$

as $n_{cl} \rightarrow n_{co}$. There are practical limitations which define the lower bound for the latter; 0.05 percent to 0.15 percent are typical values for Δ . For visible laser light, eq (6) predicts a required core diameter of a few microns. This places stringent demands on fiber technology.

A considerable amount of effort has gone into developing various descriptions of the propagation phenomena in monomode fibers and examining the relative merits and accuracies of the different material candidates for their composition. Recently, Bell Laboratories manufactured a step-index, monomode fiber of core radius $\rho = 7.3 \mu$ with the following characteristics at $\lambda = 633 \text{ nm}$,

$$\begin{aligned} NA &= 0.1159 \\ n_{co} &= 1.4631 \\ n_{cl} &= 1.4585 \end{aligned} \quad (8)$$

In this investigation, the exit end of this monomode fiber is used as the source of illumination for generating a hologram. The far-field radiation can be calculated using the Fraunhofer formula, as the fiber-end aperture is very small compared with the distance to the test surface.¹¹

The intensity distribution originating from a well prepared fiber end is nearly gaussian in shape¹²⁻¹⁴ and is similar to the gaussian spherical wave produced by a spatial filter in a conventional holographic arrangement.¹¹ The central portion of the cone of radiation provides a reasonably uniform illumination of the test surface; however, the small numerical aperture of the fiber limits the divergence of the emanating wavefront. Consequently, a monomode fiber acts like a spatial filter equipped with a low-powered microscope objective. Micro lenses can be used to collimate the beam or to produce additional beam divergence.

Fiber Bundles

Individual fibers cannot transmit images; therefore, several thousand fibers must be collected into a bundle to convey image amplitude and phase information from the test surface to the photographic plate in cases where optical access to the test surface is limited. A real image, focused on the entrance end of the bundle, can be transmitted provided that the relative orientation of each fiber in the bundle is maintained throughout its length. The bundle is classified as coherent. Each fiber transmits a different amount of light and the image at the exit end is composed of discrete components of varying intensity. Since the MMB is a light guide as opposed to a lens, a three-dimensional object must be within the depth of field of the system used to project its image onto the entrance end. The real image on the exit end can be focused on the photographic plate and superimposed with a reference wavefront to generate an image-plane hologram. The apparent proximity of the object to the plate decreases the coherence requirement on the source during reconstruction which allows a real image to be viewed in white light.^{15,16}

Although it would be desirable to use a monomode bundle for this study, all of the coherent bundles now available are composed of multimode fibers. Each fiber has a large core surrounded by a thin cladding, which makes for a very efficient MMB, since the efficiency of a fiber bundle is measured in terms of the percentage of useable transmission area and the amount of light which passes through it. On the other hand, the commercial monomode fiber used in these experiments, characterized by eq (8), has a small core and a thick cladding (about 1:12) which would make a very inefficient bundle.

Present efforts are being directed towards developing a preform using compatible glasses of similar refractive indices which, when drawn, will result in a monomode

fiber of larger core to cladding ratio to be incorporated into a highly efficient, coherent, single-mode fiber bundle or SMB.

Holographic Applications of Fiber Optics

Light emitted from the exit end of an optical fiber was used in holography as the reference wave in recording a hologram and/or the illuminating wave in reconstructing it.^{17,18} Individual fibers were also used in the object beam to illuminate the test surface. Although the problems associated with such an application have been investigated,^{19,21} object wavefronts recorded on the hologram were not captured through fiber optics and direct optical access to the test surface was required. Recently, a coherent bundle was inserted between the object and the photographic plate to convey phase information to the hologram for subsequent displacement analysis in cases where optical access was limited.⁷ These concepts were extended⁸ and displacement was measured over the full-field using coherent bundles made up from individual multimode fibers with step-index profiles or MMBs. In these deformation studies, fiber optics were used to gain access to remote areas of a structure, to reduce the number of optical components necessary for testing and to increase the flexibility of the experimental setup. Multimode fibers, however, transmit many modes, or wavefronts, which can interact during or between exposures, resulting in poor holographic recordings.

Flexible monomode fibers have not been used for holographic work due to their commercial nonavailability; however, one investigator reported launching a fundamental HE_{11} mode through a fiber designed for single-mode operation at 900 nm by careful excitation of the fiber.¹¹ Results indicated that the reduction in modal interaction eased environmental requirements for holography.

The present study used a step-index, monomode fiber designed and manufactured at Bell Laboratories for communication purposes at 633 nm. This fiber actually transmits two orthogonal polarizations of the fundamental mode which, because of noncircularity of the core or stress-induced birefringence, have slightly different propagation constants,²⁰⁻²² so there is some modal dispersion but this is a very small effect, especially in comparison with a commercial multimode fiber. A single loop can also be introduced in the fiber to suppress one

of these modes. It would be expected that by minimizing intermodal dispersion, holograms can be recorded with better diffraction efficiency and stringent requirements for vibration isolation ordinarily associated with holographic testing can be somewhat relaxed.

In holographic interferometry, two reconstructed hologram images corresponding to the undeformed and deformed test surface are superimposed. A displacement fringe pattern is observed which is governed by²³

$$(\hat{e}_1 - \hat{e}_2) \cdot \underline{d} = n\lambda \quad (9)$$

where \underline{d} is the displacement vector, n the fringe order number, λ the wavelength, and \hat{e}_1 and \hat{e}_2 are unit vectors along the directions of propagation from the source and to the observation point respectively, drawn to/from the point under consideration. In short, the observed displacement fringes are due to the change in optical-path length which occurs between exposures. These path-length changes give rise to a distribution of phase differences between the reconstructed wavefronts which results in areas of constructive or destructive interference and are seen as light and dark fringes. The component of displacement measured at each point depends upon the location of the source and on the point of observation.

The exit end of the monomode fiber which illuminates the test object acts as the source point, while the entrance end of the coherent multimode fiber bundle is at the point of observation. The assembly of rays inherent in each fiber in the imaging bundle may be described in terms of a mean path length. This is defined as the average of the path lengths for all rays weighted by their respective transmittances; respective path lengths distribute around this mean value.²⁴ The minimum and maximum optical-path length in a step-index, multimode fiber of length l are $n_{co}l$ for the ray traveling straight down the core and $(n_{co}^2/n_{cl})l$ for a ray at the critical angle, respectively. The spread of the distribution Δl , however, does not exceed $\Delta l_{max} = n_{co}(n_{co}/n_{cl} - 1)l$.

When the undeformed and deformed states of the object surface are transmitted through the coherent bundle, all of the modes experience equal changes in optical-path length for each object point focused on the entrance end. In general, however, many object points are focused on a single fiber and several phase differences are transmitted. Upon superposition, the intensity in each fiber is pro-

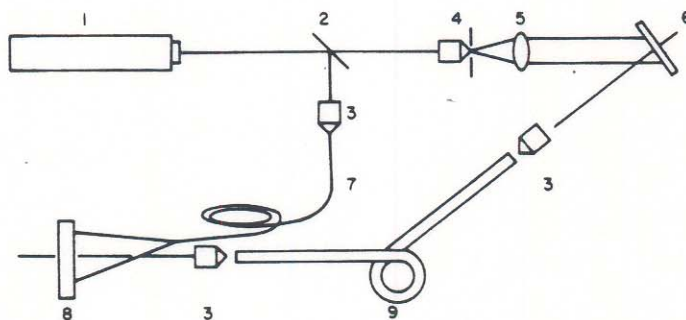


Fig. 1—The experimental setup

1. C.W. LASER; 2. BEAM SPLITTER; 3. MICROSCOPE OBJECTIVES;
4. BEAM EXPANDER & SPATIAL FILTER; 5. COLLIMATING LENS;
6. PHOTOGRAPHIC PLATE (HOLOGRAM); 7. SINGLEMODE OPTICAL FIBER;
8. TEST OBJECT; 9. COHERENT MULTIMODE OPTICAL FIBER BUNDLE.

portional to the mean displacement over the core and the overall image includes a fringe pattern governed by eq (9).

Experiments

Experiments were initially carried out to demonstrate the feasibility of using the monomode fiber characterized by eq (8) to illuminate two- and three-dimensional test surfaces for holographic deformation analysis. Additional tests, some of which were carried out using an individual multimode fiber for comparison purposes, showed the monomode fiber to be clearly superior for holographic recording, primarily because vibration-isolation requirements became less stringent. In all tests, real images of the test surfaces were transmitted to the hologram through a 2-mm diameter, MMB capable of resolving 27 line pairs/mm and composed of individual 12- μ diameter fibers.

As shown in Fig. 1, the monomode fiber was situated with its exit end parallel to the entrance end of the MMB. A reference wavefront recorded the phase changes which occurred between exposures. The surface of a clamped centrally loaded circular disk of 7.62-cm diameter was positioned normal to the fiber optics at a sufficiently large distance so that the displacement-phase relation governed by eq (9) reduces to

$$W = \frac{n\lambda}{2} \quad (10)$$

where λ is the wavelength, n the fringe order number and W is the displacement component measured along the line of sight.

A He-Ne laser, $\lambda = 633$ nm, was used to record a hologram of the undeformed disk on a photographic

plate. The center of the disk was displaced under load 3.81×10^{-3} cm along the line of sight and a hologram of the deformed surface was recorded, superimposed on the initial hologram. Figure 2 shows the white-light reconstruction of the processed double-exposure hologram with the resulting fringe pattern corresponding to displacement measured normal to the plane of the clamped disk. The jagged appearance of the displacement fringes can be attributed to the manner in which the individual fibers in the MMB convey phase information and to the density and construction of the MMB itself.⁸ The deflection of the disk at a distance r from the center is given by²³

$$W = \frac{Pr^2}{8\pi D} \log \frac{r}{a} + \frac{P}{16\pi D} (a^2 - r^2) \quad (11)$$

where

$$D = \frac{Eh^3}{12(1-\nu^2)} \quad (12)$$

Equations (11) and (12) are for a disk of radius a and thickness h with Young's modulus and Poisson's ratio of E and ν , respectively. The load, P , was determined from the change in deflection of the center of the disk imposed between exposures. Figure 3 shows a computer generated plot of the fringe loci predicted for our experiment in which

$$\begin{aligned} a &= 3.81 \text{ cm} & E &= 27.58 \times 10^5 \text{ kPa} \\ h &= 0.318 \text{ cm} & \nu &= 0.35 \end{aligned} \quad (13)$$

Light, integer fringes in Fig. 2 agree well with the theoretical fringe loci.

A similar test involving a three-dimensional subject was conducted using a cylindrical pipe of length L . The pipe was rigidly fixed at end $Z/L = 0$ and a torque was applied at $Z/L = 1$, to produce a state of pure torsion. Z is measured along the longitudinal axis of the pipe from

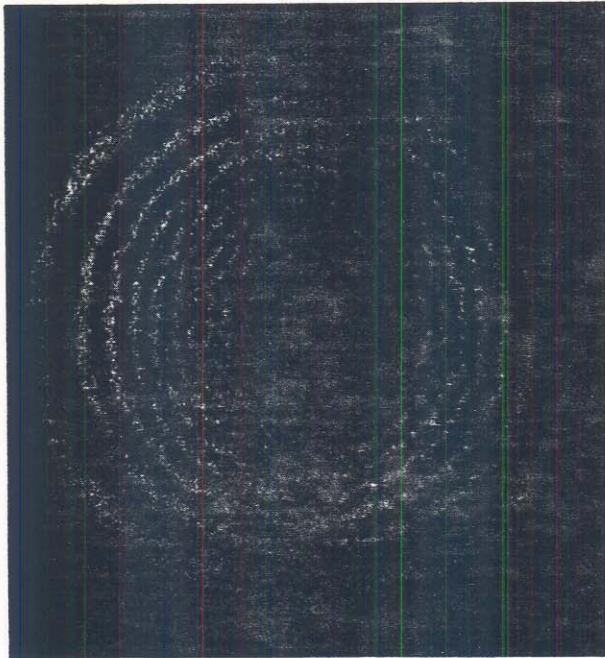


Fig. 2—Displacement pattern of a centrally loaded clamped circular disk using an individual monomode fiber for illumination and a multimode coherent bundle of 12- μ diameter fibers for image transmission

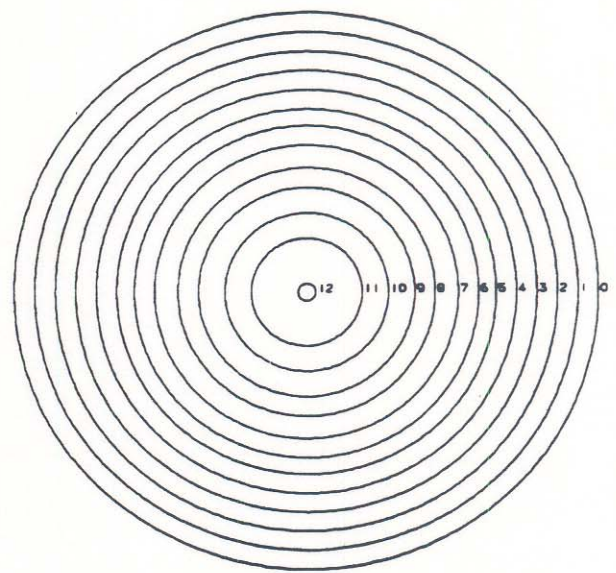


Fig. 3—Computer-generated plot of theoretical fringe loci for the centrally loaded clamped circular disk

the fixed support towards the end at which the torque, M_T , is applied. The surface of the pipe was within the depth of field of the lens system used to project its image on the entrance end of the coherent bundle. This ensured that all points of the image projected on the photographic plate were in focus. Figure 4 shows the fringe pattern measured along the line of sight, that is perpendicular to the plane of the figure in the region $0 \leq Z/L \leq 1/2$.

The tangential component of displacement is given by²⁶

$$U_\theta = \frac{d_o}{2} \phi(Z) \quad (14)$$

where d_o is the outer diameter of the pipe and $\phi(Z)$ is the angle of twist. The latter is given by

$$\phi(Z) = \frac{64 M_T (1 + \nu) Z}{\pi [d_o^4 - d_i^4] E} \quad (15)$$

In eq (15), d_i is the inner diameter of the pipe, ν the Poisson's ratio, and E is the Young's modulus.

The displacement along the line of sight is

$$W = U_\theta \cos \theta = \frac{d_o}{2} \phi(Z) \cos \theta \quad (16)$$

where θ is the radial coordinate. Figure 5 shows the theoretical fringe loci in the region $0 \leq Z/L \leq 1/2$; $0 \text{ deg} < \theta < 180 \text{ deg}$, for this experiment in which

$$\begin{aligned} M_T &= 0.38 \text{ Nm} & E &= 27.58 \times 10^5 \text{ kPa} \\ d_o &= 4.85 \text{ cm} & \nu &= 0.37 \\ d_i &= 4.06 \text{ cm} & L &= 17.78 \text{ cm} \end{aligned} \quad (17)$$

The fringe patterns in Figs. 4 and 5 agree well with each other at points removed from the fixed constraint. Careful examination of the pattern shown in Fig. 4 reveals some fringes on the support frame, indicating that deformation and/or rigid-body motion occurred in this region. If effectively rigid, the entire support would be completely free of fringes.

The two tests described above were repeated using an individual multimode fiber to illuminate the test surfaces for comparison purposes. Reconstructions were of comparable quality to those shown in Figs. 2 and 4, provided

that the fiber remained stationary during and/or between exposures.

Additional stability tests were performed using the monomode and then the multimode fiber for illumination. In these tests, the illuminating fiber was modulated during and between exposures using air currents from a small fan. Only the ends of each fiber were constrained. There was no noticeable effect on the holographic recordings for the monomode fiber; however, no reconstructions were obtained when the modulated multimode fiber was used for illumination. We therefore conclude that monomode fibers are clearly superior for holographic recording, primarily because vibration-isolation requirements become less stringent with the decrease in modal interaction.

Discussion and Conclusion

Holographic deformation fringes on the centrally loaded clamped circular disk and at points removed from the fixed support on the torsion specimen agreed well with theory. Unexpected deformation and/or rigid-body motion at the fixed end of the torsion specimen was revealed by the presence of fringes on the supporting structure. In general, fringe patterns obtained on these flat and curved surfaces are of better quality than those previously obtained using multimode fiber bundles to illuminate the object^{7,8} and diffraction efficiency is not affected by modulations in the illuminating fiber during and/or between exposures. Further improvements in fringe quality will be made when the monomode fiber bundle becomes available.

The basic characteristics of radiation relevant to holography are coherence, the form of the wavefronts and polarization. Wavefronts of laser light maintain their coherence properties even after extreme distortions by random media; consequently, for the most part coherence is preserved in the wavefronts transmitted through fiber optics and both multimode and monomode fibers can be used as coherent light guides for holography. It has been shown, however, that a holographic reconstruction becomes brightest when the object and reference wavefronts are linearly polarized perpendicular to the plane containing their axes of propagation.²⁷ The polarization in the multimode coherent bundle used for this investi-

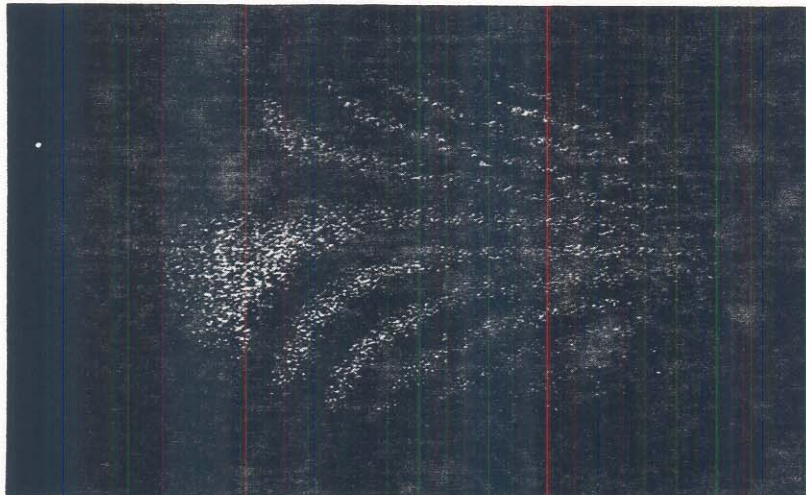


Fig. 4—Displacement pattern of a pipe subjected to pure torsion using an individual monomode fiber for illumination and a multimode coherent bundle of 12- μ diameter fibers for image transmission

gation is distributed at random throughout the radiation pattern due to scattering within the fibers and to the fact that each guided mode has its own polarization state. The polarization of coherent light passing through monomode fibers can be controlled to some degree and has been studied by several investigators.^{21,22,23} The sole guided mode really corresponds to two modes having the same configuration but with orthogonal polarizations.⁵ Coupling often occurs between these modes and light becomes elliptically polarized. Linearly polarized light can be obtained by modifying the fiber profile, for example, using an elliptical core,²⁷ or more readily by bending the fiber into a specified radius. The latter can be accomplished with very little effort and very little penalty. This may, however, induce mechanical stress which could affect other transmission characteristics of the fiber.³⁰ These would have to be taken into consideration if the configuration of the bend were modified during or between exposures.

Initial feasibility studies carried out with the setup shown in Fig. 1 have shown that vibration isolation is not required at the test site provided that the laser, launching optics and photographic plate are isolated on a vibration-free table. A monomode fiber bundle further increases optical stability by decreasing modal interaction and allows displacement to be measured in remote areas of a structure, potentially at locations removed from the laboratory. In some cases, this may require a second monomode fiber in the reference beam to keep the object and reference path lengths within the coherence length of the laser, but really represents no problem.

In conclusion, monomode fibers are well suited for holographic deformation studies and will serve as valuable new tools for the experimental stress analyst.

Acknowledgment

Research was supported by the Army Research Office (Grant No. DAAG-29-80-K-0028) and Bell Laboratories. Special thanks are extended to R.D. MacDougall and K.F. Leeb of American Cystoscope Makers, Inc., for their cooperation and interest in the project and to J.H.

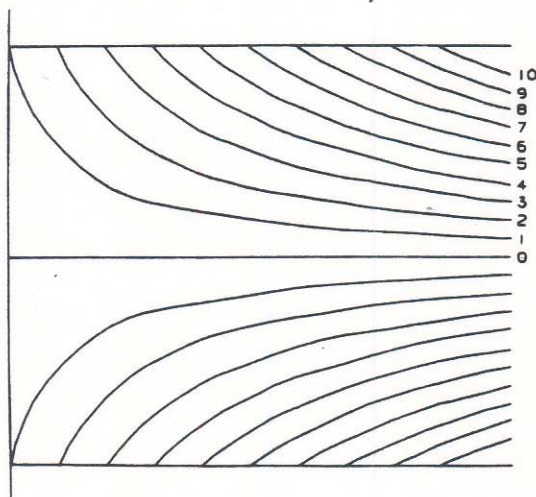


Fig. 5—Computer-generated plot of theoretical fringe loci for the pipe subjected to pure torsion

Bennewitz for his help in preparing the figures for the paper.

References

1. Miller, S.E. and Chynoweth, A.G., editors, *Optical Fiber Telecommunications*, Academic Press, New York, San Francisco, London (1979).
2. Collin, R.E., *Field Theory of Guided Waves*, McGraw-Hill, New York (1960).
3. Kapany, N.S. and Burke, J.J., *Optical Waveguides*, Academic Press, New York (1972).
4. Marcuse, D., *Light Transmission Optics*, Van Nostrand, New York (1972).
5. Marcuse, D., *Theory of Dielectric Optical Waveguides*, Academic Press, New York (1974).
6. Pask, C., Snyder, A.W. and Mitchell, D.J., "Number of Modes on Optical Waveguides," *J. Opt. Soc. Amer.*, **65** (15), 356-357 (March 1975).
7. Gilbert, J.A. and Herrick, J.W., "Holographic Displacement Analysis with Multimode Fiber Optics," *EXPERIMENTAL MECHANICS*, **21** (8), 315-320 (Aug. 1981).
8. Gilbert, J.A., Schultz, M.E. and Boehnlein, A.J., "Remote Displacement Analysis Using Multimode Fiber Optic Bundles," *Proc. SESA Spring Meeting*, Dearborn, MI, 41-43 (May 1981).
9. Marcuse, D., "Loss Analysis of Single-Mode Fiber Splices," *Bell Syst. Tech. J.*, **56** (5), 703-718 (May 1977).
10. Gloge, D., "Weakly Guiding Fibers," *Appl. Opt.*, **10** (10), 2252-2258 (Oct. 1971).
11. Leite, A.M.P.P., "Optical Fibre Illuminators for Holography," *Opt. Comm.*, **28** (3), 303-308 (March 1979).
12. Peterman, K., "Fundamental Mode Micro Bending Loss in Graded Index and W Fibers," *Opt. Quantum Electron.*, **9** (2), 167-175 (Feb. 1977).
13. Gambling, W.A. and Matsumura, H., "Propagation in Radially Inhomogeneous Single-Mode Fibers," *Opt. Quantum Electron.*, **10** (1), 31-40 (Jan. 1978).
14. Marcuse, D., "Gaussian Approximation of the Fundamental Modes of Graded Index Fibers," *J. Opt. Soc. Amer.*, **68** (1), 103-109 (Jan. 1978).
15. Sciammarella, C.A. and Chawla, S.K., "A Lens Holographic-moire Technique to Obtain Components of Displacement and Derivatives," *EXPERIMENTAL MECHANICS*, **18** (10), 373-381 (Oct. 1978).
16. Gilbert, J.A. and Exner, G.A., "Holographic Displacement Analysis Using Image-plane Techniques," *EXPERIMENTAL MECHANICS*, **18** (10), 382-388 (Oct. 1978).
17. Suhara, T., Nishihara, H. and Koyama, J., "The Far Field Patterns of the Light Emitted from a Fiber and Their Application to Holography," *Proc. Annual Meeting of IECE of Japan*, S15-2 (in Japanese) (March 1975).
18. Suhara, T., Nishihara, H. and Koyama, J., "Analysis of the Radiation Characteristics of Optical Fibers for the Hologram Reconstruction," *Report of Fukusha - Kagaku Kenkyukai* (in Japanese) (Dec. 1974).
19. Suhara, T., Nishihara, H. and Koyama, J., "Far Radiation Field Emitted from an Optical Fiber and Its Application to Holography," *Trans. of the IECE of Japan*, **E60** (10), 533-540 (Oct. 1977).
20. Rashleigh, S.C. and Ulrich, R., "Polarization Mode Dispersion in Single-mode Fibers," *Opt. Lett.*, **3** (2), 60-62 (Aug. 1978).
21. Ramaswamy, V., Standley, R.D., Sze, D. and French, W.G., "Polarization Effects in Short Length, Single-mode Fibers," *Bell Syst. Tech. J.*, **57** (3), 635-651 (March 1978).
22. Ramaswamy, V. and French, W.G., "Influence of Non-circular Core on Polarization Performance of Single Mode Fibers," *Elect. Lett.*, **14** (5), 143-144 (March 1978).
23. Sollid, J.E., "Holographic Interferometry Applied to Measurements of Small Static Displacements of Diffusely Reflecting Surfaces," *Appl. Opt.*, **8** (8), 1587-1595 (Aug. 1969).
24. Suzuki, T., "Interferometric Uses of Optical Fiber," *Japanese J. of Appl. Phys.*, **5** (11), 1065-1074 (Nov. 1966).
25. Timoshenko, S. and Woinowsky-Krieger, S., *Theory of Plates and Shells*, McGraw-Hill, New York (1959).
26. Timoshenko, S., *Strength of Materials*, D. Van Nostrand Co., New York (1940).
27. Rose, H.W., Williamson, T.L. and Collins, Jr., S.A., "Polarization Effects in Holography," *Appl. Opt.*, **9** (10), 2394-2396 (Oct. 1970).
28. Simon, A. and Ulrich, R., "Evolution of Polarization Along a Single-mode Fiber," *Appl. Phys. Lett.*, **31** (8), 516-520 (Oct. 1977).
29. Stolen, R.H., Ramaswamy, V., Kaiser, P. and Pleibel, W., "Linear Polarization in Birefringent Single-mode Fibers," *Appl. Phys. Lett.*, **33** (8), 699-701 (Oct. 1978).
30. Namihira, Y., Kudo, M. and Mushiaki, Y., "Effect of Mechanical Stress on the Transmission Characteristics of Optical Fiber," *Electronics and Comm. in Japan*, **60-C** (7), 107-115 (July 1977).

3.4 Holographic/Fiber Optic Experiments

Figure 3.1, excerpted from reference 42, demonstrates one set of experiments on HFO recording performed in a course on experimental mechanics taught by the writer at the University of Alabama in Huntsville. Four experiments are proposed; all involve interferometry and are designed to illustrate various methods of holographic superposition for stress analysis.

Two monomode fiber optic illuminators are prepared to illuminate the object and to act as the reference wavefront in each of the experiments. The protective coating is removed from the ends of the fiber (approximately 1") using acid, or by burning the coating with a match. Ends are prepared by initially scoring the fiber over a conventional tool bit (approximately 1/2" from the end) and then initiating a fracture by bending the tip. Differences in length between the fibers should be noted so that they can be taken into consideration when matching the pathlengths of the object and reference beams.

TECHNICAL NOTE - MULTIPLY THE LENGTH OF A FIBER BY THE INDEX OF REFRACTION OF ITS CORE TO DETERMINE THE EQUIVALENT PATHLENGTH IN AIR.

Nearly all spatial filter devices can be modified to accommodate an optical fiber. For example, a pinhole can be replaced with a magnet having a hole drilled through its center. The fiber can be fed through the hole and held in place using some epoxy or adhesive tape. A suitable alternative is to use a low power microscope objective (5X objectives will produce good results; higher powers tend to launch light outside of the numerical aperture of the fiber) and a three axis positioner. The fiber can be anchored to the positioner using a magnet coated with felt. The alternative is to purchase commercially available devices, such as fiber launchers, vacuum chucks to hold the fibers, or a directional coupler to eliminate the beam splitter. These

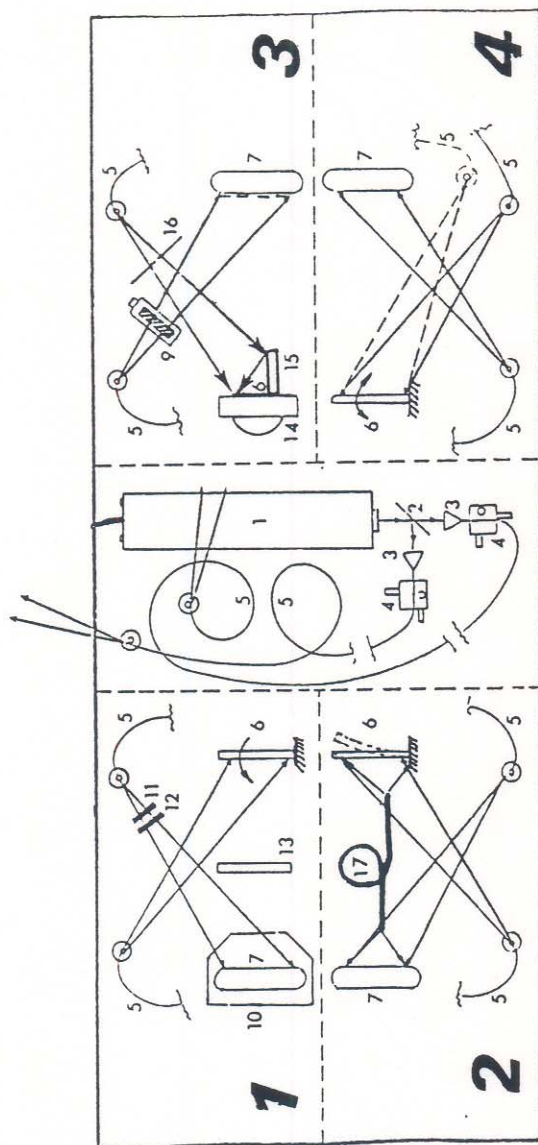


Figure 3.1 Experimental layout for holo-interferometric experiments.

Key to Figure

- | | | |
|--------------------------|---------------------------------|---------------------------------|
| 1. laser | 7. hologram | 12. polarizer in rotation mount |
| 2. beam splitter | 8. lens | 13. linear polarizer |
| 3. microscope objective | 9. grating on translation stage | 14. rotation stage |
| 4. three-axis positioner | 10. real-time device | 15. mirror |
| 5. monomode fiber | 11. adjustable half-wave plate | 16. shutter |
| 6. test object | | 17. coherent imaging bundle |

are not absolutely necessary; the procedure for aligning the configuration shown in Figure 3.1 is analogous to that used to align the pinhole in a spatial filter.

The exit ends of the two fibers can now be anchored to posts or other optical mounts (using small magnets coated with felt), providing diverging sources of coherent light that can be easily positioned throughout the working space. The advantage is that the same fibers can be used for each experiment, eliminating the need for multiple beamsplitters, spatial filters, mirrors, and lenses.

Experiment No. 1 demonstrates that real-time holographic interferometry can be accomplished by making a single holographic recording of a test piece in its rest position; the hologram is processed and replaced in its original exposed position with respect to the test piece; then the holographic image is observed to be superimposed on the object. Any subsequent movement of the test piece will produce real-time fringes. The investigator is encouraged to move the hologram, the reference beam, the illumination, or the object to illustrate that the resulting phase changes superimpose with the deformation and change fringe localization. This exercise serves as background for understanding the holographic-moire method, and visually demonstrates the principle of phase modulation which is currently used in systems for automated processing of holographic interferograms and discussed later in this chapter.

A more elaborate set-up for this experiment involves placing a linear polarizer between the object and hologram, and a linear polarizer followed by a half wave plate mounted in a rotation stage in the reference beam. The undeformed state of the object is recorded with the polarizations of both beams aligned. Real-time holographic fringes will be observed when the object is loaded, but only the undeformed state is reconstructed (the holographic

interference fringes vanish) when the polarization of the reference beam is rotated through 90 degrees. This approach has been used to holographically store information in real-time studies involving speckle photography[43], and moire interferometry[44].

Experiment No. 2 demonstrates that double-exposure holographic interferometry can be accomplished when holograms of an object in its undeformed and deformed states are superimposed. A coherent fiber bundle is used to transmit an image to the film plate. Interferometric fringes can be analyzed using phase-displacement equations.

Experiment No. 3 demonstrates that a single component of displacement can be isolated using a holographic-moire method. The model can be mounted on a rotation stage along with a mirror positioned so that the object can be illuminated from two different directions. An initial holographic recording is made with the object illuminated by the direct beam and the indirect (from the mirror) beam. The object is deformed and rotated. The interference fringes produced by each illumination superimpose to form a moire pattern indicative of the displacement component measured perpendicular to the angle bisector of the illumination in a direction parallel to the plane formed by the propagation vectors from the source to the object, and from the object to the hologram.

Two (or more) holograms can be recorded on the same photographic plate without changing the angle of illumination of the reference beam. This process is called multiplexing and can be accomplished by inserting a relatively coarse grating (10 lines/in) in the reference beam. The grating is translated through one-half the pitch between holographic recordings. Depending upon the position of the grating during reconstruction, either one

of the images or both of them can be viewed through the developed hologram. The image of the grating will not show up on a photographic recording as long as the grating is outside the depth of field of the imaging system. This process can be used in the present experiment to separately record the interference pattern produced by the direct and indirect beams if an appropriate shutter system is used to block the corresponding portion of the object beam. The moire pattern can be viewed when the grating in the reference beam is in an intermediate position, or completely removed.

Experiment No. 4 demonstrates that time-average holographic interferometry can be accomplished by recording a hologram over a period of time when the object undergoes a periodic vibratory motion. Two (or more) different modes of vibration of an object (vibrated at different frequencies) can be captured on the same plate by changing the angle of the reference beam.

3.5 Automated Analysis

One of the major factors inhibiting full exploitation of the holo-interferometric measuring technique is the difficulty of getting reliable numerical results out of the holo-interferograms. Automated quantitative evaluation of holo-interferograms requires accurate interference phase measurement for any fringe position independently of field intensity variations in the reconstructed image. Unfortunately, this presents a formidable challenge to the holographer, since real interferograms are often characterized by discontinuous, ambiguous or extraneous fringes of varying gradient and contrast, as well as an uneven background complete with speckle noise and possibly shaded by the geometry of the test surface. Consequently, a completely automated holo-interferogram analysis would most likely have to include signal averaging, spatial smoothing, normalizing to local intensity

values, provisions for subtracting off the nonuniform background, and a systematic means of resolving ambiguities.

Although there is not yet a general method available that can be used to reliably interpret any and all arbitrary holo-interferometric fringe patterns, great strides have been made in applying automated data reduction procedures to specific applications[45]. Digital processing can involve locating fringe centers, fitting interpolating functions, or otherwise preparing data to produce a point-by-point map of surface displacement if such is needed. An alternate strategy for flaw detection is to apply pattern recognition techniques to look for anomalous holo-interferometric fringe patterns.

If holo-interferometry is to be commonly used as an industrial measurement tool, some general method of simplifying the recording and analysis of complex and/or ambiguous holo-interferograms must be developed. One approach to this problem is to introduce a known carrier fringe pattern whose phase adds vectorially to the phase changes caused by the surface deformation to produce a perturbed fringe pattern with fringe orders that monotonically increase in the direction orthogonal to the carrier. To be effective, such a carrier fringe pattern must be localized on the surface of the reconstructed object. Fortunately, the issue of fringe localization in holography has been thoroughly investigated[8,12], and several schemes exist to introduce appropriately localized carrier fringes. Examples include rotation of the object, movement of the hologram or holographic plate, tilting of the object beam, and shearing of the reference wavefront. Subtraction of the carrier from the perturbed pattern aids in making peak/valley distinctions in the surface profile and unambiguously establishes the algebraic sign of the displacement vector[46-48]. References 47 and 48 follow; current status of automated analysis will be reported in the tutorial.

Automated Analysis of Holoferograms for the Determination of Surface Displacement

by D.R. Matthys, T.D. Dudderar and J.A. Gilbert

ABSTRACT—A method for using an image digitizing system with a minicomputer to automatically determine surface-displacement fields by evaluating holographic fringe patterns is presented. The problem of determining the sign of the displacement vector as well as the need to produce a monotonic phase change across the surface under observation is solved by utilizing the method of carrier fringes. A set of programs has been written so that the camera/computer system can view the pattern of deformation-modulated carrier fringes and, with a knowledge of the initial carrier-fringe pattern, draw a profile plot of the deformed surface. The procedure is exemplified with a study of a centrally loaded disk.

Introduction

Although interferometry is sometimes said to be one of the most significant applications of holography,¹ it is in fact rarely found in actual industrial settings. There are several reasons for this, including the need for vibration isolation of the system, the complexity of the required optical setup, and the problems of using a photographic darkroom process. But probably the major factor inhibiting full exploitation of holographic interferometry as a precision noncontact full-field measurement tool is the difficulty of getting quantitative results out of the interferograms.

Current developments in holographic techniques have made it possible to alleviate many of these difficulties, e.g., high-power pulsed lasers can remove the need for vibration isolation, fiber-optic cables and bundles can greatly simplify optical setups and allow holographic measurements in remote or inaccessible locations,² and special holographic cameras are now available that do not require darkroom procedures and which produce holographic images *in situ* within a few seconds.

In spite of these technical advances, quantitative holographic interferometry has not found widespread applica-

tion. The real root of the problem lies in the fact that the interference patterns obtained in practical cases are frequently so complex that a skilled analyst cannot easily derive quantitative results from them. Moreover, the interferogram does not contain sufficient information to determine the sign of a surface displacement, i.e., whether the surface has moved towards or away from the observer. Heretofore, most efforts to use digital methods in the study of holoferograms have been limited to the analysis of basically linear fringe distributions due to simple translations or nearly uniform deformations;³⁻⁷ but little effort has been directed toward solving these fundamental problems. However, if holography is to become a commonly used measurement tool, some method of simplifying the analysis of reasonably complex interferograms must be developed. The goal of the work described in this paper is to show that by combining image digitization with computerized analysis, this simplification can in fact be attained through the use of carrier fringes. The introduction of carrier fringes into holographic-interference-fringe patterns is not new;⁸⁻¹⁰ but the present work describes the successful application of sophisticated image digitization techniques, carrier fringes, fiber optics, and computer coding into a unified system for automatic fringe analysis.

The main advantages of the carrier-fringe technique are that it removes the sign ambiguity ordinarily present in interferometric fringe patterns and that it also imposes monotonicity on the phase change across an object surface so that an automated system may be used for analysis. Computer codes have been developed to analyze the fringe patterns so that it is now feasible to design a system which, given knowledge of the carrier-fringe pattern, can automatically evaluate the holoferometric fringes on the deformed surface and produce a plot of displacements of that surface.

To develop and test such an automated system, it was decided to map the surface deflection of a centrally loaded linear-elastic disk. This is a familiar test specimen. The results are known from theory; and the interference patterns obtained from such a test object are neither trivial nor excessively complex. A photograph of the interference pattern obtained by making a double-exposure hologram of a disk before and after applying central loading is shown in Fig. 1. The interference fringes are basically just a set of concentric rings. Note that it is impossible to determine the direction of surface deflection from study of the holoferogram alone. The

D.R. Matthys (SEM Member) is Associate Professor, Marquette University, Physics Department, Milwaukee, WI 53233. T.D. Dudderar (SEM Fellow) is Member of Technical Staff, AT&T Bell Laboratories, Room 1A-105, 600 Mountain Avenue, Murray Hill, NJ 07974. J.A. Gilbert (SEM Member) is Professor, University of Alabama in Huntsville, Department of Mechanical Engineering, Huntsville, AL 35899.

Paper was presented at the 1985 SEM Spring Conference on Experimental Mechanics held in Las Vegas, NV on June 9-14.

Original manuscript submitted: August 26, 1986. Final manuscript received: June 29, 1987.

disk may be bowed either inward or outward. Also, the curved fringes are difficult to interpret by automated analysis because of the problem of programming the computer to enable it to detect when the same fringe is being encountered in a different location. Unfortunately, without some method for uniquely identifying each fringe, the computer may count each of them more than once during a scan across the disk face. One method to obviate this problem (without invoking operator interaction) is to incorporate an initial carrier-fringe pattern with a higher spatial frequency than any expected from the deformation-modulated carrier-fringe pattern. Figure 2 shows the appearance of the unloaded disk when carrier fringes are created in the holographic image. In this case the fringes were generated by tilting the disk, but in fact the carrier pattern could have been generated by changing the orientation of the illumination, the reference beam, or the hologram itself.¹¹

The governing equation for holographic displacement analysis on a diffuse surface is

$$(\hat{e}_1 - \hat{e}_2) \cdot d = n\lambda \quad (1)$$

where d is the displacement vector, n is the fringe order, and λ is the wavelength. For each point on the test surface, \hat{e}_1 and \hat{e}_2 are unit vectors drawn from the source to the point and from the point to the observation position, respectively.

The quantity $(\hat{e}_1 - \hat{e}_2) \cdot d$ is often referred to as the projected displacement d_p .

The carrier pattern required for digitization can be expressed as

$$\delta = n_1\lambda \quad (2)$$

where δ is the linear phase change across the field of view and n_1 is the carrier-fringe order. To be effective these carrier fringes should be localized close to the test

surface, and oriented perpendicular to the direction of scan denoted by s .

When deformation is superimposed on the carrier, the modulated fringe pattern is given by

$$(\hat{e}_1 - \hat{e}_2) \cdot d + \delta = n_2\lambda \quad (3)$$

The fringes in the hologram corresponding to eqs (2) and (3) can be digitized and subtracted, and

$$(\hat{e}_1 - \hat{e}_2) \cdot d = (n_2 - n_1)\lambda = \Delta n\lambda \quad (4)$$

Equation (4) is the same as eq (1) when $n = n_2 - n_1$. The carrier pattern will facilitate digitization of the deformation-modulated carrier-fringe pattern when the fringe gradient of the carrier, $d(n_1)/ds$, meets certain conditions. Differentiating eq (4),

$$d(d_p)/ds = [d(n_2 - n_1)/ds]\lambda = [d(n_2)/ds - d(n_1)/ds]\lambda \quad (5)$$

In eq (5), $d(d_p)/ds$ represents the rate of change of the projected displacement, and $d(n_1)/ds$ and $d(n_2)/ds$ are the slopes of the carrier and deformation-modulated fringe patterns, respectively, in plots of fringe order versus row/column number. In general, the slope of the carrier-fringe pattern, $d(n_1)/ds$, is known, and $d(n_2)/ds$ can be measured for each point along s . This uniquely specifies $d(d_p)/ds$, and hence the sign of the projected displacement is determined. When $d(n_1)/ds > 0$, the method works provided that $d(n_2)/ds$ never becomes negative. This condition must be satisfied to insure that each fringe in the modulated pattern is scanned only once, and the modulated pattern has monotonically increasing fringe orders over the scan. This condition depends on the fringe gradient in the carrier pattern; the higher the carrier-fringe density, the less likely that

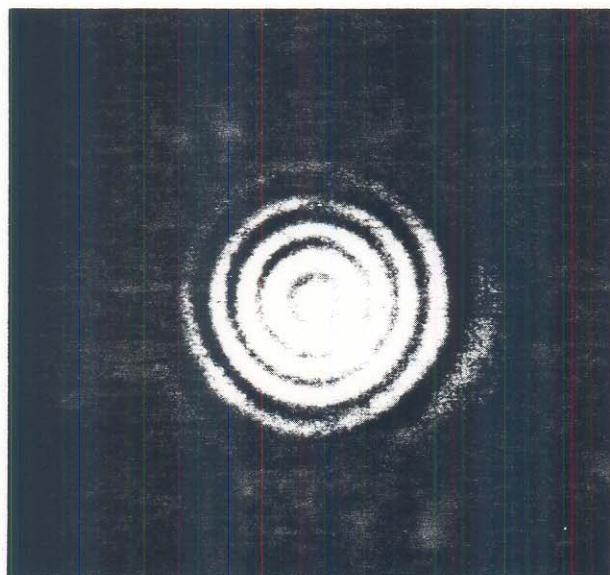


Fig. 1—Double-exposure holographic image of a disk before and after central loading showing interference fringes due to surface deformation

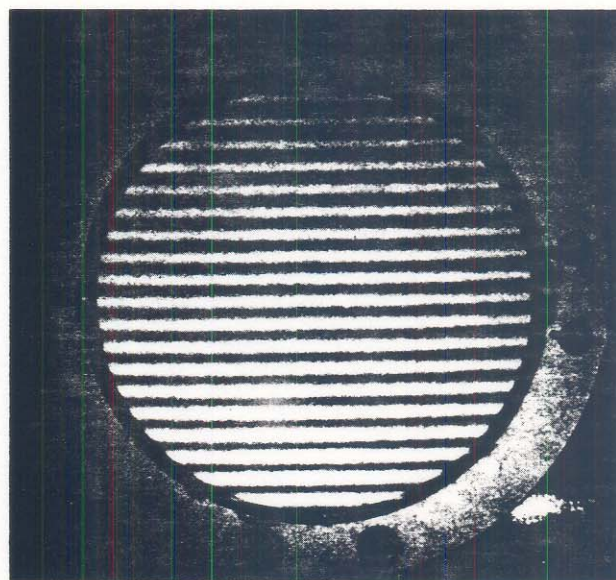


Fig. 2—Carrier-fringe pattern generated by introducing a small tilt about a horizontal diametral line across the surface of the undeformed disk. The rotation was 0.0039 deg with the bottom of the disk moving towards the observer

$d(n_2)/ds < 0$. However, the resolution of the imaging system imposes some constraints. Not only must the carrier-fringe density remain within the resolution limit, but so must that of the deformation-modulated fringe pattern.

Assigning arbitrary fringe-order numbers along a scan line uniquely establishes the sign of the projected displacement. In this case, however, the magnitude of d_p is determined to only within a constant. Absolute displacement measurement requires that absolute fringe orders be established in both the carrier and the modulated patterns. This is most easily done by initiating a known carrier thereby assigning n_1 , and then following one fringe in real time as deformation occurs to determine n_2 . An alternative method is to have prior knowledge of the displacement of at least one point in the deformation-modulated fringe field. For example, a point lying on a fixed boundary will have the same fringe order in the carrier and deformation-modulated carrier-fringe patterns.

In this experiment, the disk was tilted about a horizontal axis through the center of the disk surface, with the bottom of the disk being moved toward the observer. Since the direction of the tilt is known, the sign of the fringe orders can be assigned unambiguously; the carrier-fringe-order numbers are increasing toward the bottom of the disk and decreasing toward the top. The zero order fringe is located directly above the rotation axis.

Figure 3 shows the appearance of the fringe pattern when a holointerferogram of the disk is recorded with both carrier and deformation present. Note that no fringe appears twice when counted along a vertical line from bottom to top anywhere along the disk. The effect of the deformation fringes is to merely expand or compress the carrier-fringe spacing, so it is simple to determine whether the fringe order is increasing or decreasing. Since suitable programs are available, it is possible for the computer, equipped with a digitizing camera, to view the fringe pattern of the loaded surface and automatically draw a plot of the surface deformation of the disk.

Experimental Setup

A glass disk of 88-mm diameter and 1.6-mm thickness was bonded around its circumference to a stiff ring suspended vertically in a gimbal holder which permitted

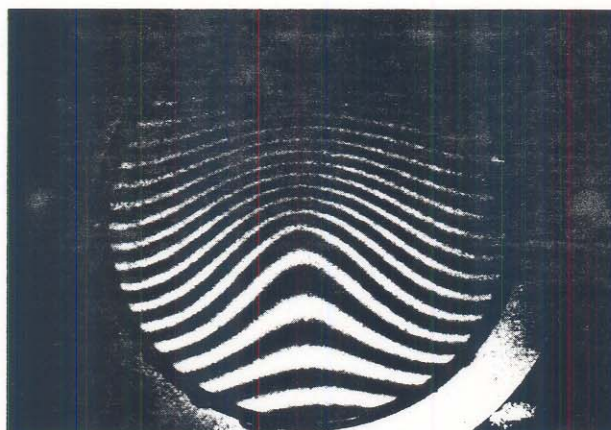


Fig. 3—Holointerferometric fringes caused by combining the carrier tilt and the deformation due to central loading of the disk. The amount of loading was 1.60 microns toward the observer

the disk to be rotated around either a vertical or horizontal axis through a surface diameter. In addition, a large micrometer was positioned behind the disk to allow the application of controlled central displacements.

Figure 4 shows the optical setup used to generate the holograms. For a symmetric arrangement with equal illumination and viewing angles (measured with respect to the surface normal), the normal displacement W is given by eq (1) which simplifies to $2W \cos \beta = n\lambda$, where β is the illumination angle, n is the fringe order, and λ is the wavelength of light used. In this test arrangement, the angle β was 4.58 degrees and the light source was a helium-neon laser, so normal or out-of-plane displacements could be measured with a fringe sensitivity of 0.317 microns. A single-mode optical fiber was used for illumination to simplify the setup.

Figure 5 is a block diagram showing the major components of the system used for this test of automated fringe reduction and surface contouring. The vidicon camera used is capable of digitizing an image with an eight-bit gray scale (256 levels) and a resolution of 1024 by

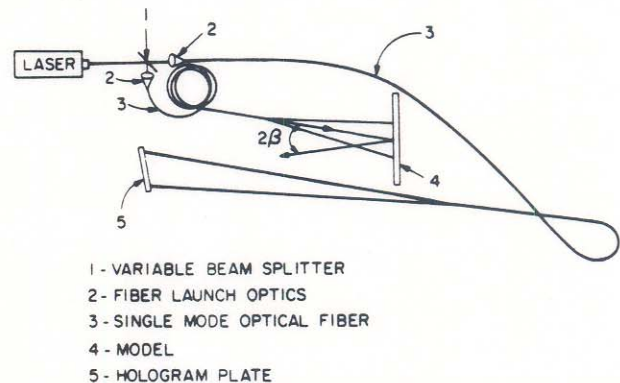


Fig. 4—Optical setup for taking holograms of the disk. The arrangement of the angle 2β between the illumination and viewing directions established the sensitivity vector as normal to the disk surface and allowed measurement of out of plane deformation. In this setup the value of β was 4.58 deg

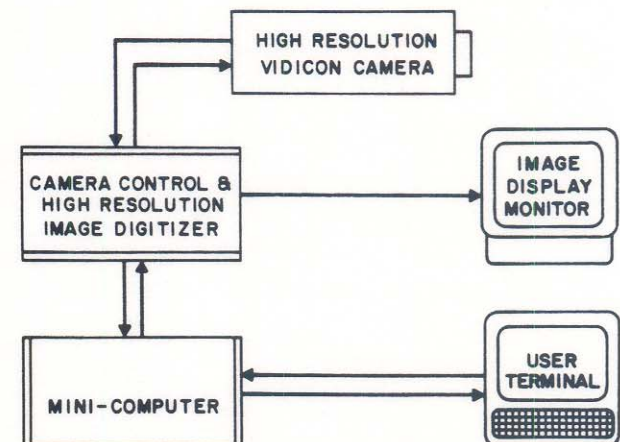


Fig. 5—Schematic showing the equipment used in the experiment

1024 pixels. A camera control allows selection of every second or every fourth row and column element, thus allowing the resolution to be reduced to 512 by 512, or 256 by 256 pixels. To reduce the size of the data files a resolution of 256 by 256 was chosen for this experiment. Consequently, the data files obtained from digitizing the holographic images were only 64K bytes in size. Such files can easily be handled by a relatively small computer, enabling the calculations involved in this experiment to be performed on a relatively inexpensive system.

Experimental Procedure

The actual data needed for this approach include only digitized holointerferometric images of (1) the unloaded disk with a carrier-fringe pattern, and (2) the loaded disk showing the deformation-modulated carrier-fringe pattern, plus knowledge of the direction of tilt used to generate the carrier-fringe pattern. Therefore the first step was to produce a suitable holointerferometric carrier pattern across the disk surface. Using a thermoplastic holocamera, a hologram was made of the unloaded disk. Then the disk was tilted 0.0039 degrees about a horizontal diametrical line across the disk surface. The direction of tilt was such that the bottom of the disk moved toward the observer. A photograph was then taken of the real-time fringe

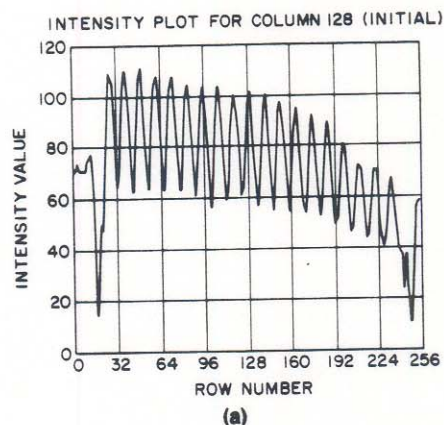
pattern generated by interference effects between the holographic image of the disk and the tilted disk surface. The resulting fringe distribution is shown in Fig. 2. The center of the disk was then displaced 1.60 microns toward the observer and another photograph of the fringe distribution on the disk surface taken. This deformation-modulated carrier-fringe pattern is shown in Fig. 3.

Data Analysis

Since the direction of tilt is known, all of the information needed to contour the deformed surface is contained in these two photographs. To enable automated analysis, the pictures were digitized using the vidicon camera as described above. The column representing the vertical center line through the disk surface, column 128 of the data arrays, was chosen to demonstrate the method of analysis.

An intensity plot of this column, scanning from bottom to top, is shown in Figs. 6(a) and 6(b) for each of the two images. Figure 6(a) shows the initial intensity variation across the unloaded, undeformed disk with its carrier fringe pattern, while Fig. 6(b) shows similar information for the loaded, deformed disk. Figure 6(a) clearly shows the edges of the disk and the basically uniform sinusoidal intensity distribution across the disk surface. In addition

Fig. 6—(a) Intensity trace across vertical midline of the disk for fringe distribution shown in Fig. 2 (carrier fringes only). Direction of scan was from the bottom edge of the disk to the top along column 128. (b) Intensity trace across vertical midline of the disk for fringe pattern shown in Fig. 3 (carrier plus deformation). Direction of the scan was from bottom to top along column 128



INTENSITY PLOT FOR COLUMN 128 (LOADED)

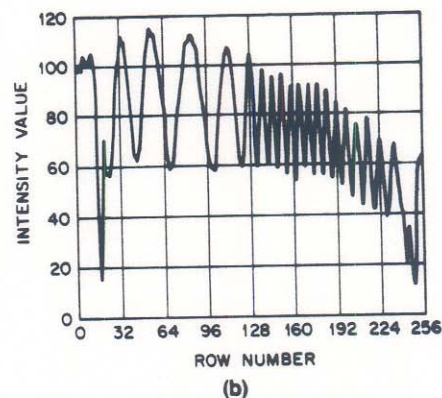
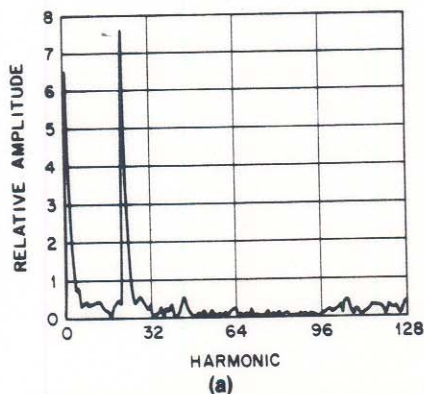
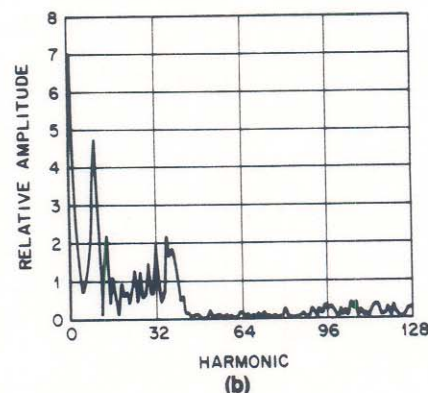


Fig. 7—(a) Spectral plot of the intensity trace given in Fig. 6(a) (carrier fringes only). The spatial harmonics were measured in terms of the 256 rows in the data array, i.e., the fundamental frequency would produce one complete cycle across the 256 rows. (b) Spectral plot of the intensity trace given in Fig. 6(b) (carrier plus deformation fringes). Spatial harmonics were measured as in Fig. 7(a)

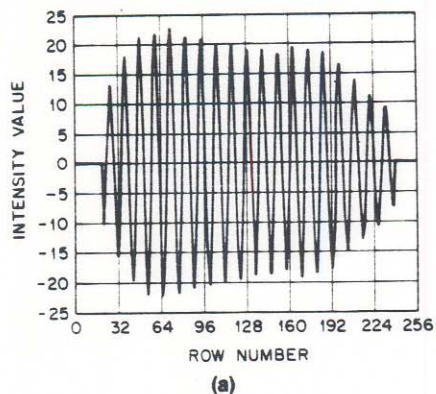
SPECTRAL PLOT FOR COLUMN 128 (INITIAL)



SPECTRAL PLOT FOR COLUMN 128 (LOADED)



SMOOTHED/FILTERED COLUMN 128 (INITIAL)



SMOOTHED/FILTERED COLUMN 128 (LOADED)

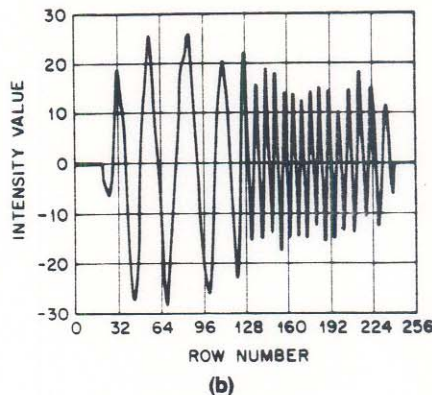


Fig. 8—(a) Filtered and smoothed version of trace given in Fig. 6(a) (carrier only). (b) Filtered and smoothed version of trace given in Fig. 6(b) (carrier plus deformation)

to the sinusoidal carrier-fringe pattern, a very low frequency intensity variation due to the Gaussian nature of the laser illumination is also evident.

The next step was to locate the edges of the disk and clip both patterns to the midpoints of the last cycle contained within these edges. Fourier transforms of the clipped patterns are shown in Figs. 7(a) and 7(b). The important characteristics of Fig. 7(a), which shows the frequency spectrum for the unloaded disk (carrier only), are the sharp peak at the carrier frequency, the very low frequency peak representing the Gaussian intensity distribution of the laser beam, and the high-frequency noise due to speckle, nonlinearities in the film, optical-system limitations, etc. Figure 7(b), which gives equivalent information for the loaded disk (carrier plus deformation), shows that the deformation information causes a frequency modulation of the original carrier pattern, with the desired information now present as a sideband of the carrier frequency. Comprehensive discussions of the use of Fourier-transform methods for the analysis of digitized holographic fringe patterns have been published by Kreis.^{12,13}

Working first with the spectrum of the undeformed image [Fig. 7(a)], the program set up a narrow passband centered around the carrier frequency. All frequencies outside this passband were removed. The program then examined the spectrum of the deformed image [Fig. 7(b)], and cut off the low-frequency spike which was the result of the Gaussian intensity envelope; it also removed all high frequencies where signal strength had fallen back to the noise level. The resulting spectra were then transformed back to the time domain using an inverse Fourier transform and the results are shown in Figs. 8(a) and 8(b). A low-frequency intensity variation still shows up as an envelope of the desired signals, but this is of minor importance since it is phase, not intensity, which is significant.

In order to find the fringes, the computer next proceeded to locate the extrema of the intensity distributions for each filtered fringe pattern. This was done by applying standard methods of data analysis¹⁴ to fit curves through the data points, and then differentiating to locate the desired extrema. Since the data for each column contain a large number of points which correspond to a small number of cycles of a basically sinusoidal intensity distribution, the graph obtained by curve fitting is relatively insensitive to the specific technique used, and any standard

DATA PLOT FOR COLUMN 128

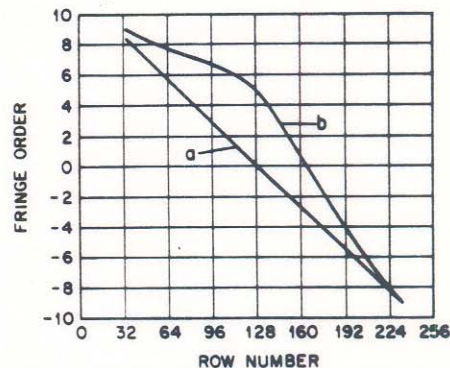


Fig. 9—Plots of the fringe order versus the row number (distance from the bottom of the disk). Curve 'a' is for the unloaded disk (carrier only), while curve 'b' is for the loaded disk (carrier plus deformation)

method should give essentially the same results. Figure 9 shows fringe-order versus row-number plots along the vertical center line (column 128) for both the unloaded and the loaded disk. The curve labeled 'a' is for the unloaded disk (carrier only) while curve 'b' is for the loaded disk (carrier plus deformation). The linear curve 'a' obtained for the unloaded case is simply a manifestation of the simple sinusoidal pattern of fringes across the face of the disk and the zero-order fringe is located at the disk center, over the rotation axis. In curve 'b', for the loaded condition, there is a slow phase change across the lower part of the disk where the intensity fringes were spaced out, and then a rapid phase change across the upper part of the disk where the fringes were crowded together.

Since curve 'a' of Fig. 9 gives information concerning the phase-change distribution due to the carrier while curve 'b' of the same figure gives the corresponding information for the deformation-modulated carrier, the next step in the process was to subtract the two curves. Since the data represent extrema occurring at different row locations in the two curves, the data will have to be interpolated first. Because the curves are smooth with respect to the spacing between data points, the choice of

interpolation method is not critical. For this experiment, a cubic-spline technique¹⁵ was used to interpolate values for each row of the two curves, and these values were then subtracted from each other to get the distribution of phase change due to the deformation alone. In addition, a phase change of zero was imposed at the edges of the disk where the disk was bonded to its support ring. This result is shown in Fig. 10, which is a profile plot of the out-of-plane deformation of the disk surface across the vertical center line from bottom to top.

Automated repetition of the preceding analysis for each digitized column provides a full-field description of the out-of-plane deformation of the disk as desired. This final result is given in Fig. 11, which shows a perspective plot of the deformed disk obtained from the computer-graphics output.

Summary

The method of carrier fringes was successfully applied in this study of a centrally loaded disk. The carrier fringes resolved the problem of sign ambiguity and linearized the fringes so that the phase shift across the disk surface was monotonic, thus allowing automatic scanning. Computer programs incorporating Fourier-transform filtering were written to analyze the holointerferometric fringes on the surface of the loaded disk. Since the computer knew the details of the carrier pattern, it was possible for the computer to draw a profile plot of the out-of-plane deformation.

The method could be extended to dynamic studies if a high-speed camera were available. Though the time required for analysis of each image precludes real-time studies of dynamic changes, a high-speed camera could be used to record the changing fringes and selected frames could be digitized and studied later. Note that the carrier image information need be given to the computer just once, and all other images need only contain information about the deformation-modulated carrier-fringe patterns.

Acknowledgments

Major funding for this work was provided by the U.S. Army Research Office under Contract Nos. DAAG 29-84-K-0183, DAAG 29-84-G-0045 and DAAL 03-86-K-0014. The authors also wish to thank AT&T Bell Laboratories, Murray Hill, NJ for its support.

References

1. Jones, R. and Wykes, C., "Holographic and Speckle Interferometry," 64, Cambridge Press, New York (1983).
2. Dudderar, T.D. and Gilbert, J.A., "Real-Time Holographic Interferometry through Fiber Optics," *J. Phys. Eng.: Sci Instr.*, **18**, 39-43 (1985).
3. Katzir, Y., Glaser, I., Friesem, A.A. and Sharon, B., "On-Line Acquisition and Analysis for Holographic Nondestructive Evaluation," *Opt. Eng.*, **21**, 1016-1021 (1982).
4. Hot, J.P. and Durou, C., "System for the Automatic Analysis of Interferograms Obtained by Holographic Interferometry," *SPIE 2nd European Cong. on Optics Applied to Metrology*, **210**, 144-151 (1979).
5. Lamy, F., Liegeois, C. and Meyrueis, P., "Automatic Computer Analysis of Double Exposure Holograms in Industrial Nondestructive Control," *Proc. SPIE*, **353**, 82-89 (1983).
6. Kreis, T.M. and Kreitlow, H., "Digital Processing of Holographic Interference Patterns," *OSA/SESA Topical Mtg. on Hologram Interferometry and Speckle Metrology*, Cape Cod, MA, Paper No. TuB2 (June 1980).
7. Lanzl, F. and Schluter, M., "Microprocessor-Controlled Hologram Analysis," *IEEE 5th Int. Computing Conf.*, London, 159-162 (1978).
8. Katzir, Y., Friesem, A.A., Glaser, I. and Sharon, B., "Holographic Nondestructive Evaluation with On-Line Acquisition and

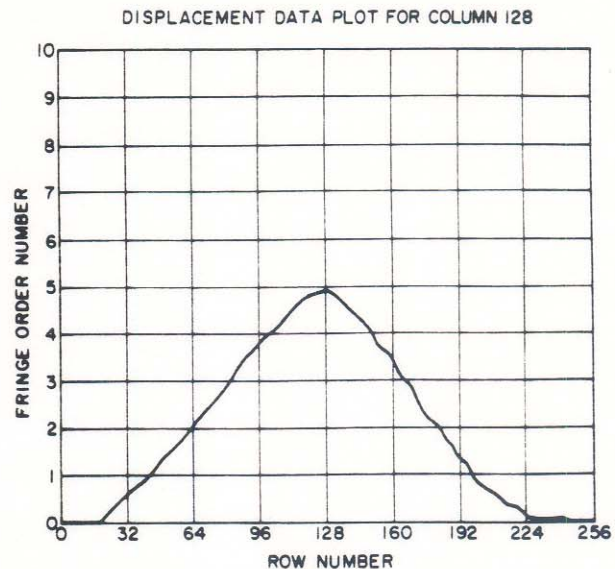


Fig. 10—Contour map of the disk surface across the vertical center line of the disk, obtained by subtracting the fringe-order distributions shown in Fig. 9(a) and 9(b)

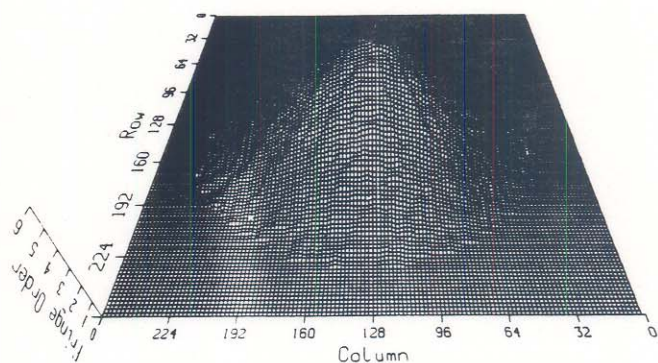


Fig. 11—Perspective plot of the out of plane displacement as derived directly from the computer-plotter output

- Processing," *Industrial and Commercial Applications of Holography*, ed. M. Chang, *Proc. SPIE*, **353**, 74-81 (1982).
9. Sciammarella, C.A. and Ahmadshahi, M., "Computer Based Method for Fringe Pattern Analysis," *Proc. 1984 SEM Fall Conf. on Exp. Mech.*, Milwaukee, WI, 61-69 (1984).
10. Plotkowski, P.D., Hung, Y.Y., Hovanesian, J.D. and Gerhart, G., "Improved Fringe Carrier Technique for the Unambiguous Determination of Holographically Recorded Displacements," *Opt. Eng.*, **24**, 754-756 (1985).
11. Beranek, W.J. and Bruinsma, A.J.A., "Geometrical Approach to Holographic Interferometry," *EXPERIMENTAL MECHANICS*, **20** (9), 289-300 (1980).
12. Kreis, T., "Digital Holographic Interference-Phase Measurement Using the Fourier-transform Method," *J. Opt. Soc. Amer.*, **A3** (9), 847-855 (1986).
13. Kreis, T. and Jüptner, W., "Digital Processing of Holographic Interference Patterns Using Fourier Transform Methods," *Measurements, J. Int. Meas. Conf., IMEKO Symp. on Laser Applications in Precision Measurements*, Budapest (1986).
14. Savitzky, A. and Golay, J.E., "Smoothing and Differentiation of Data by Simplified Least Squares Procedures," *Anal. Chem.*, **36**, 1627-1639 (1964).
15. Akima, H., "New Method of Interpolation and Smooth Curve Fitting Based on Local Procedures," *J. ACM*, **17** (4), 589-602 (1970).

A Windowing Technique for the Automated Analysis of Holo-Interferograms

D. R. Matthys,^a J. A. Gilbert,^b T. D. Dudderar^c
and K. W. Koenig^a

^a Physics Department, Marquette University, Milwaukee WI 53233, USA,

^b Department of Mechanical Engineering, University of Alabama in Huntsville, Huntsville, Alabama 35899, USA and ^c AT&T Bell Laboratories, Murray Hill, New Jersey 07974, USA

(Received 22 January 1987; revised version received 24 August 1987; accepted 25 August 1987)

ABSTRACT

A systematic method for measuring surface deformations is described which includes the use of real-time holographic interferometry, the incorporation of a carrier fringe pattern to achieve fringe linearization, and the application of image digitization and automated computer analysis for rapid quantitative interpretation. In this method, regions of interest can be selected by the use of a windowing technique in which the operator specifies the desired subregion. The problem of correctly numbering fringes which originate or vanish at the boundary where the scanning begins is solved by an algorithm which ensures correct identification of the fringe orders. The output includes a perspective plot of the out-of-plane deformation field.

This method is demonstrated by its application to a measurement of the out-of-plane deformation of a hermetically sealed plastic housing loaded by internal pressurization.

INTRODUCTION

Although interferometry is sometimes said to be one of the most significant applications of holography, it has not yet found widespread practical application. The major factor inhibiting full exploitation of the technique is the difficulty of getting quantitative results from holographic interferograms. Indeed, by itself the interferogram does not even contain sufficient information to determine the direction or sign of the surface displacement component being measured. However,

123

Optics and Lasers in Engineering 0143-8166/88/003-50 © Elsevier Applied Science Publishers Ltd, England, 1988. Printed in Northern Ireland

the real difficulty is that in practical cases the interference patterns obtained are frequently so complex that, even if the signs of the displacements were known, a skilled analyst could obtain quantitative results only with the expenditure of considerable time and effort. Therefore, if holo-interferometry is to be commonly used as a measurement tool, some method of simplifying the analysis of interferograms must be developed. This simplification can be attained through image processing and computer analysis.

Early efforts to use digital methods in the study of holo-interferograms were limited to linear fringe distributions.¹⁻³ Analysis of more complex displacements required the introduction of carrier fringes. This procedure was suggested by several investigators,⁴⁻⁶ and has been used by the authors for semi-automatic analysis of deflection (out-of-plane displacement).⁷

This paper discusses the measurement of surface deflections induced by internal pressure variations on a hermetically sealed package used to house microelectronic components. The results obtained show that a high level of automation can be achieved by using a photoelectronic-numerical system for analysis of real-time holographic interferograms. At the same time, problems resulting from geometrical discontinuities on the surface or abrupt changes in reflectivity indicate a need for the development of more sophisticated numerical algorithms before arbitrary surfaces can be fully analyzed. However, even if a particularly complex surface cannot be studied as a whole, the use of a windowing technique allows subregions of interest to be selected and analyzed.

THEORY AND BACKGROUND

Most holo-interferometric fringe patterns obtained in practical applications are too complex to be readily amenable to automated analysis. However, a carrier fringe pattern may be used to achieve fringe linearization.⁴⁻⁷ This technique involves superimposing a known linear phase shift on the phase changes caused by surface deformation to produce a monotonically changing phase distribution across the interferogram. In this way, the complex fringes of the original interferogram are reduced to 'nearly straight' fringes on which the deformation is superimposed as a modulation. Such fringes can easily be read in by a machine vision system. When the carrier fringes are later subtracted, the original information about the deformation is retrieved. In addition, the known phase characteristics of the carrier allow unambiguous determination of the sign of the displacement vector.

The use of single mode optical fibers for object and reference beam illumination greatly simplifies the required experimental set-up for conventional holographic and *holographic interferometric* applications.⁸ When coupled with modern 'instant' holographic recording systems, optical fibers provide a powerful new tool for optical measurement.⁹

A *holographic interferometric* fringe pattern can be related to the deformation of the surface by the simple vector expression

$$n\lambda = \mathbf{g} \cdot \mathbf{d} \quad (1)$$

where n is the fringe order number, λ is the wavelength of the coherent light used to record and reconstruct the hologram, \mathbf{g} is the sensitivity vector ($\mathbf{e}_2 - \mathbf{e}_1$), where \mathbf{e}_1 and \mathbf{e}_2 are unit vectors in the illumination and observation directions respectively, and \mathbf{d} is the displacement vector at the point of observation on the surface of the sample. When a relatively flat surface is intentionally oriented normal to the angle bisector of \mathbf{e}_1 and \mathbf{e}_2 , the interferometer senses only the out-of-plane displacement component, W , and eqn (1) becomes

$$n\lambda = 2W \cos \beta \quad (2)$$

where 2β is the angle between the propagation vectors in the direction of illumination and observation. A carrier pattern can be superimposed on this deformation to allow the fringe pattern to be sufficiently simplified for digital recording. Equation (2) characterizes the deflection when the carrier pattern is recorded separately and numerically subtracted from the superimposed deformation.

The surfaces best suited to automated analysis are reasonably well behaved, relatively flat, and of nearly uniform reflectance. Unfortunately, in most real problems the surfaces of interest move in a very complex manner, have irregular surface contours, and exhibit non-uniform reflectance.

FEASIBILITY STUDIES

In prior related research, the basic functionality of an automated holographic recording and analysis system was demonstrated by its application to a study of the problem of a centrally loaded disk clamped around its boundary. Figure 1a shows a conventional *holographic interferometric* fringe pattern for an edge-clamped, centrally loaded disk, as well as the *holographic interferometric* fringe patterns obtained when the disk was rotated while in the unloaded state to produce a carrier fringe pattern (Fig. 1b) and then centrally loaded to produce a perturbed



Fig. 1. (a) A *holographic interferometric* fringe pattern on the surface of a centrally loaded disk with no carrier fringes (no rotation). (b) A *holographic interferometric* carrier fringe pattern on the surface of an unloaded, undeformed disk subjected to a pure rotation. (c) A *holographic interferometric* fringe pattern on the surface of a centrally loaded disk. The fringes here are a combination of a carrier pattern produced by rotation and a deformation pattern due to the central loading.

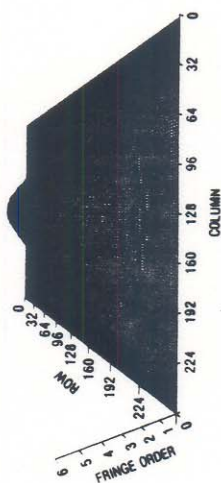


Fig. 2. A perspective plot of the deflection of the centrally loaded disk, obtained by fully automated analysis of the fringe patterns shown in Figs 1b and 1c.

or modulated carrier fringe pattern (Fig. 1c). Finally, Fig. 2 shows a plot of the surface deflection of the disk obtained by a completely automated processing of the holo-interferograms of Figs. 1b and 1c.⁷ In this case, the edge of the specimen was fixed, which greatly simplified the identification of absolute fringe orders.

The next stage in developing this process was to apply it to a component with less constrained boundaries. A package used to house microelectronic circuit cards was used for this demonstration. This housing is made from two thin plastic shells sealed together along their edges, producing a hollow container about 9.0 cm long by 5.0 cm wide by 1.2 cm thick, suitable for holding an electronic circuit card. A photograph of the top surface of this housing is shown in Fig. 3a. It was aligned in the holo-interferometer shown in Fig. 4 so that the out-of-plane displacement could be measured (using eqn (2)) with a fringe sensitivity of $0.317 \mu\text{m}$ ($\beta = 4.58^\circ$). The illuminating and reference beams were guided through single mode optical fibers.

The housing was fitted with an air valve and rubber hose so that surface deformations could be produced by elevating the internal pressure, and then mounted on a rotation stage to allow generation of the carrier pattern. Using a thermoplastic holocamera a hologram was made of the package, and then the package was rotated 0.0114° about a horizontal axis so that the top of the package moved toward the observer. A photograph was then taken of the real-time fringe pattern caused by interference between the wavefront from the holographic image of the package and the wavefront from the actual package. The internal pressure of the package was elevated and another photograph of the real-time fringe distribution was taken. These photographs are shown in Figs 3b and 3c. A simple holo-interferogram of the same deformation field is shown in Fig. 3d for purposes of comparison.

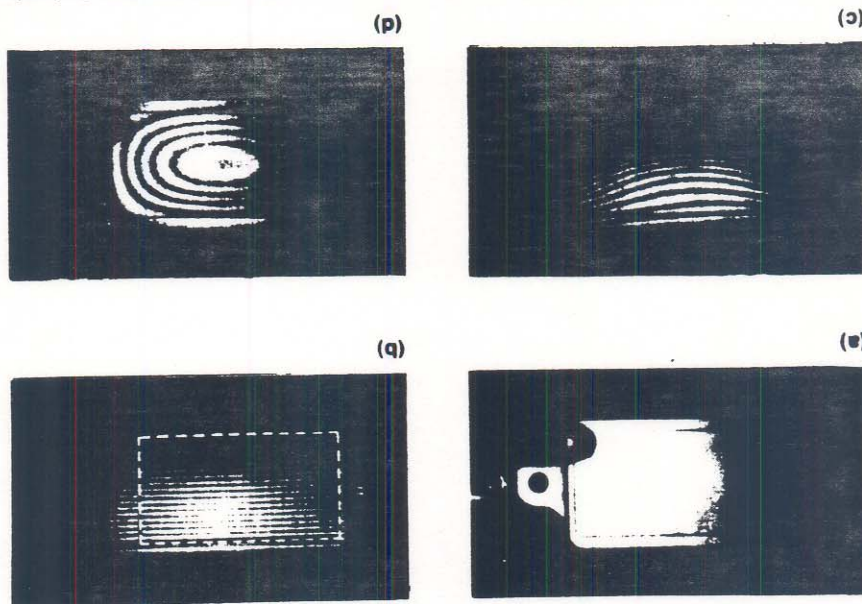


Fig. 3. (a) Photograph of the hermetically sealed housing used in the experiment. The dotted lines show the location of the area selected for analysis. (b) A holo-interferometric carrier fringe pattern produced by rotating the housing around a horizontal axis with the top moving toward the observer. (c) The carrier fringe pattern shown in Fig. 3 modulated by the surface deflections caused by a change in internal pressure. The housing was not rotated so there are no carrier fringes. (d) A deflection fringe pattern caused by a change in internal pressure.

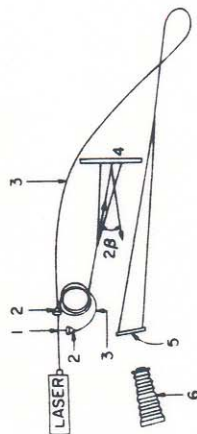


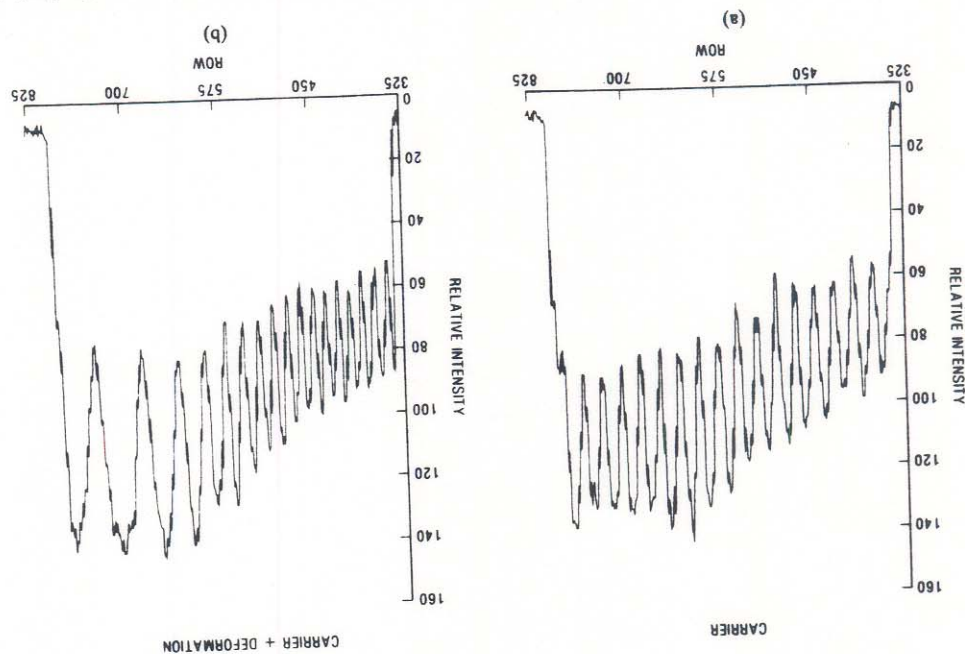
Fig. 4. A real-time holographic/fiber optic recording system. 1, variable beam splitter; 2, fiber launch optics; 3, single mode optical fiber; 4, model; 5, hologram plate; 6, camera system.

METHOD OF ANALYSIS

Since the direction of rotation of the housing is known, all the information needed to contour the deformed surface is contained in these two photographs. The contour analysis is begun by digitizing the holo-interferometric images shown in Figs 3b and 3c. The pictures were digitized using a vidicon camera with a resolution of 1024×1024 pixels and a grey scale range of 256 levels. It was decided to perform the analysis first along the vertical centerline of the surface, so for both photographs the intensity values of column 512 were selected out of the data arrays. Plots of these values are shown in Fig. 5. Various methods have been proposed for determining the phase change from such intensity plots. One common method is to transform to the Fourier domain and determine phase by analyzing the real and imaginary parts of each complex Fourier component.^{5,10,11} In this paper, however, the Fourier analysis is used only to determine the carrier frequency and to remove noise from the signal. The phase is determined by curve fitting and interpolation techniques applied in the real domain. The details of the method follow.

The values from the undeformed image (Fig. 5a) were put through a fast Fourier transform to find the carrier frequency and all other frequencies were removed. The resulting data were then transformed back to the spatial domain using an inverse fast Fourier transform to obtain a smooth intensity distribution showing the basic carrier frequency. The data from the deformed image (Fig. 5b) were also transformed with a fast Fourier transform and the knowledge of the carrier frequency obtained from the undeformed image was used to set a bandpass filter to remove noise from the data. The filtered data were then transformed back to the spatial domain as a smooth intensity distribution showing the combined results of the carrier and deforma-

Fig. 5. (a) Intensity distribution for column 512 from data array of housing with carrier fringes only. (b) Intensity distribution for column 512 from data array of housing with fringes due to both carrier and deformation



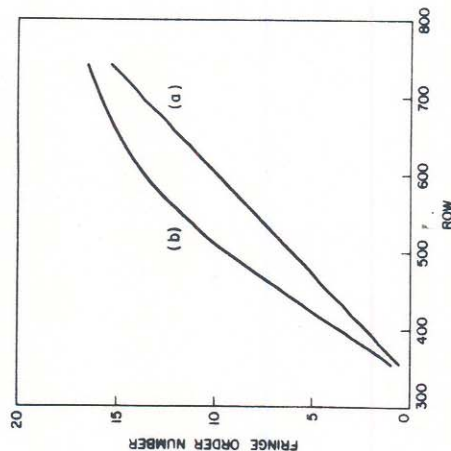


Fig. 6. Fringe order plots of (a) the carrier, and (b) the carrier plus deformation, along the vertical centerline of the hermetically sealed housing (column 512).

tion fringe patterns. In order to determine the fringe orders, the computer next proceeded to locate the extrema of the intensity distributions for each filtered fringe pattern. This was done by applying standard methods of data analysis¹² to fit curves through the data points, and then differentiating to locate the desired extrema. Figure 6 shows fringe order versus row number plots along the vertical centerline for both the unloaded and the loaded housing. Curve 'a' is for the unloaded housing (carrier only) while curve 'b' is for the loaded housing (carrier plus deformation). The linear curve 'a' obtained for the unloaded case is simply a manifestation of the simple sinusoidal pattern of fringes across the face of the housing. In curve 'b', for the loaded condition, there is a rapid phase change across the lower part of the housing where the intensity fringes were crowded together, and then a slow phase change across the upper part where the fringes were spaced out.

Since curve 'a' of Fig. 6 gives information concerning the phase change due to the carrier while curve 'b' of the same figure gives the corresponding information for the carrier plus deformation, the next step in the process was to subtract the two curves. A cubic spline technique¹³ was used to interpolate values for each row of the two curves, and these values were then subtracted from each other to get

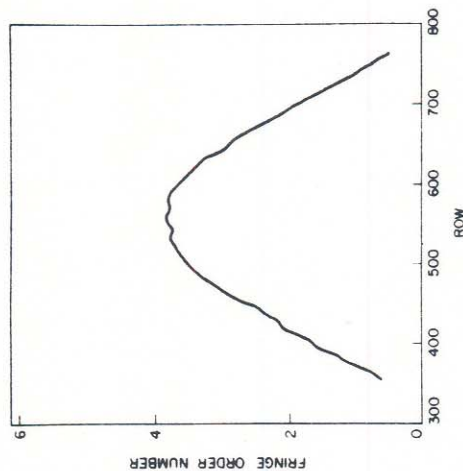


Fig. 7. Fringe order plot corresponding to the deflection along the vertical centerline of the housing (column 512).

the distribution of phase change due to the deformation alone. This result is shown in Fig. 7, which is a plot of the out-of-plane deformation of the surface across the vertical centerline from the bottom to the top of the housing as oriented in Fig. 3.

WINDOWING

An attempt to apply the above process to obtain the deflection across the entire specimen immediately showed a major limitation of the automated fringe analysis. The main problem was that surface ridges near the boundaries of the specimen introduced very rapid fluctuations in the fringes which prevented the automated system from performing valid analysis. In order to simplify the analysis and solve this problem, a method of windowing the data field was developed. This method has a number of advantages. First, it allows the user to select a subregion of interest from a larger array of data. If desired, this subregion can be magnified by zooming in on the desired region as described below. Also, the process permits the analysis of a multilevel surface where ridges and/or shadows cause discontinuities in the holographic fringe pattern. Finally, the windowing technique can be used to

effectively eliminate regions of the digitized data that may cause difficulty or be incorrectly interpreted by the scanning algorithm.

If no magnification of the subregion is desired, one can easily create a window in the original array of digitized data by simply resetting all rows and columns outside the desired region to zero. A short program was written which allowed the determination of the boundaries of the window from a video display of the digitized image. Of course, the same window must be used on both the carrier and carrier plus deformation data arrays. The window chosen here is indicated by the dotted lines in Fig. 3b, where the top, bottom and left borders were chosen to eliminate surface ridges from the area to be analyzed. The vertical border on the right was selected to eliminate the air valve with its rubber hose from the region to be analyzed. Note that the asymmetry in the final plot shown in Fig. 9a is due to the fact that the left edge of the plot corresponds to an area of the housing near one of its sealed edges, whereas the right edge of the plot represents an area of the housing closer to the center of the unit. The deformation near the center is of course considerably greater than the deformation near the edge. This is also clearly shown in Fig. 8, where the four graphs represent the surface deflection at different columns spaced across the housing surface. Very little deflection is observed in column 48, near a sealed edge, while a large deflection is found at column 512, which is

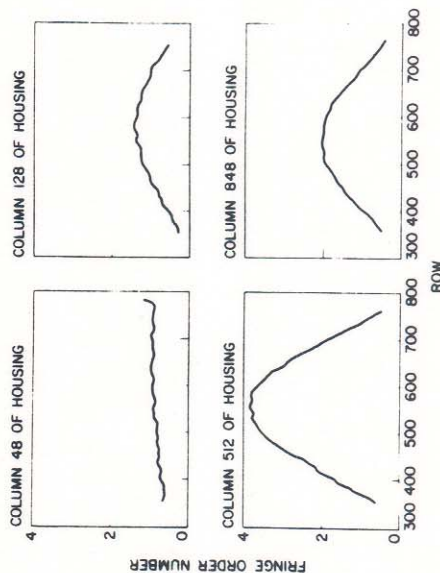


Fig. 8. Graphs of the surface deflection at various columns across the surface of the housing.

approximately the middle of the surface. Column 848 shows that the deflection is decreasing as the right window boundary is approached.

If it is desired to obtain a magnified image of a subregion, the camera can be zoomed in on the selected region, and the window borders can be specified later by mathematically resetting to zero all rows and columns outside the desired area.

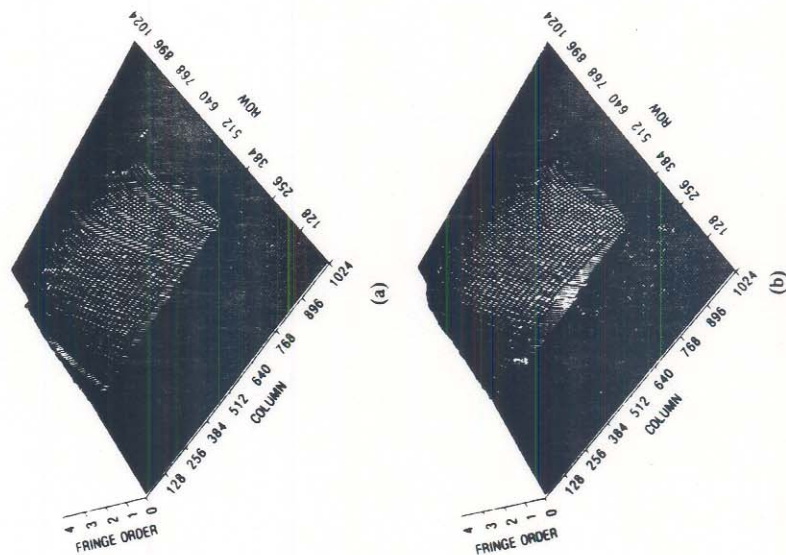


Fig. 9. (a) Plot of the surface deflection of the housing for the subregion outlined with dashed lines in Fig. 3b. The irregularities in the surface are due to errors in fringe counting. (b) Plot of the surface deflection of the housing for the subregion outlined with dashed lines in Fig. 3b. To obtain this plot, an improved fringe counting algorithm was used which monitored the gain or loss of fringes at the bottom boundary.

FRINGE COUNTING

A second problem arose because of difficulties in automatically assigning fringe orders. The successful use of the windowing technique depends on the development of an algorithm which can properly compensate for the gain or loss of a fringe along the window boundary where scanning begins. Sudden changes in the fringe count due to the gain or loss of a fringe resulted in discontinuities in the final plot. An example of such a faulty plot is shown in Fig. 9a. The solution to this problem is to make use of the nearly linear (slowly varying) character of the fringe field. Discontinuities in the deformation field between the first fringe and the window boundary are taken to signal the gain or loss of a fringe and an appropriate adjustment to the fringe count is made automatically. Fig 9b shows a plot of results from the same data used in Fig. 9a, as analyzed with a modified program containing the improved fringe count compensating algorithm.

CONCLUSION

A method for automating the measurement of complex deformations has been developed. In earlier work involving a centrally loaded disk with a clamped boundary, excellent results were easily obtained, since the disk had fixed boundary conditions and a flat surface with relatively uniform reflectivity. However, in the case of the sealed housing experiment described in this paper, problems due to surface irregularities and fringe discontinuities at the edges of the specimen posed problems. These were overcome by the use of a windowing technique together with an improved fringe counting algorithm. The basic reason that these successful results were obtained from a very simple technique was the introduction of the carrier which produced a smooth monotonic phase variation creating nearly straight fringes with a large number of data points per fringe. This allowed simple curve fitting routines to be used in determining the location of the fringes and thus determine the phase at each point. On the other hand, the Fourier transform techniques alluded to earlier do not require any curve fitting but introduce the need for 'phase-unwrapping'¹⁰ procedures. Both techniques face the same problem in establishing a proper fringe count at the boundaries.

ACKNOWLEDGEMENTS

The authors wish to acknowledge the support of AT&T Bell Laboratories, Murray Hill, NJ, Marquette University, and the University of

Alabama in Huntsville. Since 1980, Professor Gilbert's efforts in holography have been supported in part by contracts DAAG 29-84-K-0183, DAAG 29-84-G-0045 and DAAL 03-86-K-0014 with the Army Research Office in Research Triangle Park, NC.

REFERENCES

1. F. Lanzl and M. Schultze, Microprocessor-controlled hologram analysis, *IEEE 5th International Computing Conference*, London, 1978, pp. 159-62.
2. J. P. Hot and C. Durou, System for the automatic analysis of interferograms obtained by holographic interferometry, *SPIE 2nd European Congress on Optics Applied to Metrology* 210, 1979, pp. 144-51.
3. F. Lamy, C. Liegeois and P. Meyrueis, Automatic computer analysis of double exposure holograms in industrial nondestructive control, *Proc. SPIE*, 353 (1983) 82-9.
4. Y. Katzir, A. A. Friesem, I. Glaser and B. Sharon, Holographic nondestructive evaluation with on-line acquisition and processing, *Industrial and Commercial Applications of Holography*, Milton Chang (ed.), *Proc. SPIE*, 353 (1982) 74-81.
5. C. A. Sciammarella and M. Ahmadshahi, Computer based method for fringe pattern analysis, *Proc. of the 1984 SEM Fall Conference*, Milwaukee, WI, 1984, pp. 61-9.
6. P. D. Plotkowski, Y. Y. Hung, J. D. Hovanesian and G. Gerhart, Improved fringe carrier technique for unambiguous determination of holographically recorded displacements, *Opt. Engng*, 24 (1985) 754-6.
7. D. R. Matthys, T. D. Dudderar and J. A. Gilbert, Automated analysis of holo-interferograms for determination of surface displacements, *Exp. Mech.* (in press).
8. J. A. Gilbert, T. D. Dudderar, M. E. Schultz and A. J. Boehnlein, The monomode fiber—a new tool for holographic interferometry, *Exp. Mech.*, 23 (1983) 190-5.
9. T. D. Dudderar and J. A. Gilbert, Real-time holographic interferometry through fiber optics, *J. Phys. E: Sci. Instrum.*, 18 (1985) 39-43.
10. M. T. Takeda, H. Ina and S. Kobayashi, Fourier-transform method of fringe-pattern analysis for computer-based topography and interferometry, *J. Opt. Soc. Am.*, 72 (1) (1982) 156-60.
11. T. Kreis, Digital holographic interference-phase measurement using the Fourier-transform method, *J. Opt. Soc. Am. A*, 3 (1986) 847-53.
12. A. Savitzky and J. E. Golay, Smoothing and differentiation of data by simplified least squares, *Analyt. Chem.*, 36 (1964) 1627-39.
13. H. Akima, New method of interpolation and smooth curve fitting based on local procedures, *J. ACM* 17(4) (1970) 589-602.

3.6 Hybrid Analysis - Combining Holographic Interferometry with Finite Element Analysis

Contemporary methods of stress analysis for complex structural components generally fall into the area of either experimental techniques (strain gaging, moire analysis, holographic interferometry, speckle metrology, photoelasticity, etc.) or numerical techniques (finite difference, finite elements, boundary integral methods, etc.). Each approach to stress analysis has distinct strengths and weaknesses. Experimental methods generally measure (to within some experimental error) one type of unknown (either displacement, strain or stress), but further analysis (differentiation, integration, or introduction of material properties) is required to completely determine each of the others. Numerical methods, on the other hand, can completely determine all unknowns through complex mathematical routines but require an accurate knowledge of geometry, loading, and material properties. When loading and geometry become complicated, the model may neglect important factors which significantly influence the behavior of the structure.

In cases where a prototype actually exists, a combination of holographic interferometry and finite element analysis, which are in many ways complementary, can render their respective strengths more effective, and reduce, if not eliminate, their individual weaknesses. Potentially, this approach can enhance efficiency by (1) significantly reducing computational requirements, and (2) providing a much closer match to the actual boundary conditions as defined by loading the prototype structure. Moreover, such hybrid techniques may yield solutions where neither experimental nor analytical methods alone will succeed. Additional information on this approach will be given in the tutorial.

CHAPTER 4 - THE FUTURE OF HOLOGRAPHIC NON-DESTRUCTIVE EVALUATION

Most of the developmental research in holographic interferometry has been conducted under laboratory conditions. More recently, however, the technique has attracted the attention of the industrial sector and substantial efforts have been directed toward making holographic measurements under "field" conditions[9,16,49,50]. The ideal industrial holographic measurement system should be robust enough to be transported by road, lift, crane, etc. to its point of operation without becoming misaligned, flexible enough to enter regions with limited access, and capable of being rapidly modified to meet unexpected requirements. Operation should be possible under adverse environmental conditions, response time should be immediate, and most importantly, results should be readily interpretable by a user relatively unfamiliar with the technology underlying the system.

A decade ago, these requirements could not have been met. Lasers were fragile and sensitive to changes in their operating environments; holographic systems had to be located on an isolated optical bench and were constructed using a multitude of mirrors, beamsplitters, lenses, and spatial filters; measurements were influenced by fluctuations in optical path caused by changes in the surrounding environment; real-time recording was messy and time consuming, requiring a wet cell complete with repositioning micrometers; and, quantitative results were usually extracted by photographing holograms from selected observation positions, scanning the photographs for fringe locations, and manually feeding this information to a mainframe computer programmed for single or multiple hologram analysis. Results were usually presented in tabular form and computer graphics were rarely incorporated into postprocessing.

In short, holographic interferometry was limited in reaching its full potential in the industrial sector largely because of a lack of proper tools and equipment necessary to record and develop holograms, and the inability to quickly access and properly interpret the complicated interference patterns that arise in most practical applications. Other factors which have led to slow industrial acceptance of holographic non-destructive testing include the relatively high cost per hologram, dissatisfaction with reliability and field servicing of lasers, laser safety regulations, the normally slow acceptance rate of new technology, the time consuming process of designing new test procedures for a specific application, and in some cases, the need for a highly skilled operator.

The future for industrial holo-interferometry looks very bright, mainly because support has been, and is being, provided for the high-risk/high-payoff ventures required to bring this area of technology to its full potential. Recent advances in equipment and image processing have overcome many of the technical difficulties associated with the holographic recording process, greatly expanding the range of potential applications of holo-interferometry in an industrial environment. Holocameras are now available with rapid in situ processing which greatly facilitates whole-field studies of deformation in real time. The resulting holo-interferometric fringes can be recorded digitally and, with the use of a carrier fringe technique, may soon be interpreted automatically and unambiguously. Single mode optical fibers can be used as stable illuminators in any holo-interferometer, and it is only a matter of time before a coherent single mode optical fiber bundle becomes available, allowing tests to be performed on remote objects using rugged, compact holographic probes.

Acknowledgements

The author would like to thank Rudy Garza of Newport Corporation for providing supplementary material for the tutorial. Many of the ideas incorporated in this presentation were based on joint research conducted with Dr. T. D. Dudderar of AT&T Bell Laboratories and Professor D. R. Matthys of Marquette University. During the period 1980-87, the author's efforts in holography and holo-interferometry were supported in part by contracts DAAG 29-80-K-0028, DAAG 29-84-K-0183, DAAG 29-84-G-0045, and DAAL 03-86-K-0014, administered by Dr. Edward Saibel and Dr. Robert Singleton of the Army Research Office in Research Triangle Park, N.C. The holographic techniques developed during that period are currently being applied to study thermal-mechanical deformations in printed wiring boards with funding provided by the Alabama Research Institute under contract 5-31682, and to study crystal growth under microgravity conditions with funding provided by MSFC/NASA under contract NAS8-36620.

REFERENCES

1. Gabor, D., "Nature", A new microscopic principle, 161, (1948), pp. 777-778.
2. Leith, E. N., Upatnieks, J., Wavefront reconstruction with continuous tone objects, J. Opt. Soc. Amer., 53, (1963), pp. 1377-1381.
3. Collier, R. J., Burckhardt, C. B., Lin, L. H., Optical Holography, Academic Press, N.Y., (1971).
4. Caulfield, H. J., Handbook of Optical Holography, Academic Press, N.Y., (1979).
5. Abramson, N., The Making and Evaluation of Holograms, Academic Press, N.Y., (1981).
6. Taylor, C. E., Holography - Chapter VII in the Manual on Experimental Stress Analysis, ed. by A. S. Kobayashi, Society for Experimental Mechanics, (1978).
7. Erf, R. K., Holographic Nondestructive Testing, Academic Press, N.Y., (1974).
8. Vest, C. M., Holographic Interferometry, Wiley Publishers, N.Y., (1979).
9. Ebbeni, J., Industrial Applications of Holography, Proceedings SPIE, Vol. 349, (1982).
10. Powell, R. L., Stetson, K. A., Interferometric analysis by wavefront reconstruction, J. Opt. Soc. Am., 55, (1965), pp. 1593-1598.
11. Stetson, K. A., Powell, R. L., Interferometric hologram evaluation and real time vibration analysis of diffuse objects, J. Opt. Soc. of Am., 55, (1965), pp. 1694-1695.
12. Stetson, K. A., A rigorous theory of the fringes in hologram interferometry, Optik, 29, (1970), pp. 386-400.
13. Hung, Y. Y., Taylor, C. E., Measurement of surface displacements normal to the line of sight by holo-moire interferometry, J. Appl. Mech., 42, (1975), pp. 1-4.
14. Sciammarella, C. A., Gilbert, J. A., A holographic-moire technique to obtain separate patterns for components of displacement, Exp. Mech., 16, (1976), pp. 215-220.
15. Dandliker, R., Thalmann, R., Heterodyne and quasi-heterodyne holographic interferometry, Optical Engineering, 24, 5, (1985), pp. 824-831.
16. Tozer, B. A., Glanville, R., Gordon, A. L., Little, M. J., Webster, J. M., Wright, D. G., Holography applied to inspection and measurement in an industrial environment, Optical Engineering, 24, 5, (1985), pp. 746-753.

17. Camatini, E., Optical and Acoustical Holography, Plenum Press, N.Y., (1972).
18. Gilbert, J. A., Dudderar, T. D., Applications of fiber optics to coherent metrology for the study of material deformations and structural mechanics, Proceedings of the Army Symposium on Solid Mechanics, Advances in Solid Mechanics for Design and Analysis, (1984), pp. 63-92.
19. Stimpfling, A. Smigielski, P. New method for compensating and measuring any motion of three-dimensional objects in holographic interferometry, Optical Engineering, 24, 5, (1985), pp. 821-823.
20. Pryputniewicz, R. J., Time average holography in vibration analysis, Optical Engineering, 24, 5, (1985), pp. 843-848.
21. Nishida, N., Sakaguchi, M., Saito, F., Holographic coding plate: a new application of holographic interferometry, Appl. Opt., 12, 7, (1973).
22. Rosen, A. N., Holographic funduscopy with fiber optic illumination, Opt. and Laser Tech., 7, 3, (1975).
23. Hadbawnik, D., Holographische endoskopie, Optik, 45, 1, (1976), pp. 21-38.
24. Suhara, T., Nishihara, H., Koyama, J., Far radiation field emitted from an optical fiber and its application to holography, Trans. of the IECE of Japan, Sec E (Engl), 60, 10, (1977), pp. 533-540.
25. Leite, A. M. P. P., Optical fiber illuminators for holography, Opt. Commun., 28, 3, (1979), pp. 303-306.
26. Yonemura, M., Nishisaka, T., Machida, H., Endoscopic hologram interferometry using fiber optics, Appl. Opt., 28, 9, (1981), pp. 1664-1667.
27. Dudderar, T. D., Gilbert, J. A., Fiber optic pulsed laser holography, Appl. Phys. Lett., 43, 8, (1983), pp. 730-732.
28. Gilbert, J. A., Herrick, J. W., Holographic displacement analysis with multimode-fiber optics, Exp. Mech., 21, 8, (1981), pp. 315-320.
29. Gilbert, J. A., Schultz, M. E., Boehnlein, A. J., Remote displacement analysis using multimode fiber-optic bundles, Exp. Mech., 22, 10, (1982), pp. 398-400.
30. Gilbert, J. A., Dudderar, T. D., Schultz, M. E., Boehnlein, A.J., The monomode fiber-a new tool for holographic interferometry, Exp. Mech., 23, 2, (1983), pp. 190-195.
31. Rowley, D., The use of a fiber-optic reference beam in a focused image holographic interferometer, Opt. and Laser Tech., 15, 4, (1983), pp. 194-198.

32. Gilbert, J. A., Dudderar, T. D., Nose, A., Remote deformation field measurement through different media using fiber optics, 24, 4, (1985), pp. 628-631.
33. Dudderar, T. D., Gilbert, J. A., Boehnlein, A. J., Achieving stability in remote holography using flexible multimode image bundles, Appl. Opt., 22, 7, (1983), pp. 1000-1005.
34. Gilbert, J. A., Dudderar, T. D., Boehnlein, A. J., Ultra low-frequency holographic interferometry using fiber optics, Opt. and Lasers in Eng., 5, 1, (1984), pp. 29-40.
35. Jones, J. D. C., Corke, M., Kersey, A. D., Jackson, D.A., Single-mode fiber-optic holography, J. Phys. E: Sci. Instrum., 17, (1984), pp. 271-273.
36. Dudderar, T. D., Gilbert, J. A., Franzel, R. A., Schamell, J. H., Remote vibration measurement by time averaged holographic interferometry, Exp. Tech., 9, 1, (1985), pp. 25-27.
37. Hall, P. M., Dudderar, T. D., Argyle, J. F., Thermal deformations observed in leadless ceramic chip carriers surface mounted to printed wiring boards, IEEE Trans., CHMT-6, 4, (1983), pp. 544-552.
38. Dudderar, T. D., Gilbert, J. A., Real-time holographic interferometry through fiber optics, J. Phys. E: Sci. Instrum., 18, (1985), pp. 39-43.
39. Dudderar, T. D., Hall, P. M., Gilbert, J. A., Holo-interferometric measurement of the thermal deformation response to power dissipation in multilayer printed wiring boards, Exp. Mech., 25, 1, 1985, p. 95-104.
40. Albe, F., Holographie ultra-rapide utilisant des fibres optiques, Report R 101/86, Institut Franco-Allemand de Recherches de Saint-Louis, (1986).
41. Albe, F., Fagot, H., Smigielski, Use of an endoscope for optical fiber holography, Proceedings of the SPIE 2nd. Int. Tech. Sym. on Optical and Electro-Optical Applied Sci. and Eng., Cannes, France, December, (1985).
42. Gilbert, J. A., Displacement analysis using holographic interferometry, Proceedings of the 1986 Spring Conference on Experimental Mechanics, Society for Experimental Mechanics, New Orleans, LA, June 1986, pp. 185-191.
43. Chiang, F. P., Li, Q. B., Real-time laser speckle photography, Applied Optics, 23, (1984), pp. 4469.
44. Johnson, H. S., Gilbert, J. A., Matthys, D. R., Dudderar, T. D., Real-time moire interferometry, Proceedings of the Spring Conference on Experimental Mechanics, Society for Experimental Mechanics, New Orleans, LA, June 1986, pp. 964-970.
45. Trollinger, J. D., Automated data reduction in holographic interferometry, Optical Engineering, 24, 5, (1985), pp. 840-842.

46. Plotkowski, P. D., Hung, Y. Y., Hovanesian, J. D., Gerhart, G., Improved fringe carrier technique for unambiguous determination of holographically recorded displacements, *Optical Engineering*, 24, 5, (1985), pp. 754-756.
47. Matthys, D. R., Dudderar, T. D., Gilbert, J. A., Automated analysis of holo-interferograms for the determination of surface displacement, *Experimental Mechanics*, 28, 1, (1988), pp. 86-91.
48. Matthys, D. R., Gilbert, J. A., Dudderar, T. D., A windowing technique for the automated analysis of holo-interferograms, *Optics and Lasers in Engineering*, 8, 2, (1988), pp. 123-136.
49. Dudderar, T. D., Gilbert, J. A., Matthys, D. R., Potential applications of fiber optics and image processing in industrial holo-interferometry, *Proceedings of the SPIE*, Vol. 746, *Industrial Laser Interferometry*, (1987), pp. 20-28.
50. Parker, R. J., Jones, D. G., Holography in an industrial environment, *Optical Engineering*, 27, 1, (1988), pp. 55-66.